Advancement towards the experimental measurement of the LBE thermal properties using DSC technique

Satya Prakash Saraswat[a*], Nicola Forgione[a], Massimo Emilio Angiolini[b]

[a]*DICI Department, University of Pisa, Italy,*

[b]*ENEA FSN-ING-SIS, ENEA CR Brasimone, Località Brasimone, 40032 Camugnano (BO), Italy*

Abstract

The differential scanning calorimetry (DSC) method has recently emerged as a sophisticated and precise technique for promising contributions to the thermal analysis of various materials, including heavy liquid metal (HLM) coolants. However, there is a lack of experimental studies on the thermal properties of lead-based fluids, such as lead-bismuth eutectic (LBE) and lead-lithium eutectic, which are potential candidates for use as coolants, breeders, and neutron multipliers in advanced nuclear systems like the fourth-generation lead-cooled fast reactor.

The available experimental data on the thermal properties of LBE and other lead-based fluids is limited, and the measurements have significant uncertainty. In addition, the composition of components used in the previous studies is inconsistent, and the environmental conditions were often unknown. Therefore, to fill these gaps and advance the thermal properties measurement technique for heavy liquid metal coolants, ENEA Brasimone, in collaboration with DICI-UNIPI, has installed a DSC instrument setup.

The experiments performed at the installed DSC setup are focused on measuring some essential thermal properties of LBE using DSC. The experience gained from this work will facilitate the measurement of other fluids based on lead alloy, especially lead-lithium eutectic, a potential candidate for breeder, coolant, and neutron multiplier in DEMO fusion reactors. This study represents the first effort to advance the DSC approach for accurately measuring the thermal characteristics of heavy liquid metals that are highly reactive, such as lead-lithium, which has significant potential in advanced nuclear systems.

keywords: *lead-bismuth eutectic (LBE), Differential Scanning Calorimetry (DSC), liquid-metals, melting point, latent heat of melting, solidification point, latent heat of solidification, and specific heat capacity.*

Highlights:

- *lead-bismuth thermal properties for adapting system codes to conduct the safety analysis.*
- *Differential Scanning Calorimetry (DSC) and its scope in the measurement of thermal properties of liquid-metals*
- *database for lead-bismuth eutectic thermal- properties*
- *building platform to correctly measure the thermal characteristics of liquid metals that are very reactive, such as lead-lithium.*

Acknowledgements

This work has been carried out within the framework of the HORIZON2020, Call H2020-MSCA-IF-2020, funded by the European *Research Executive Agency* (REA) *via the Marie Skłodowska-Curie Actions (Grant Agreement No 101030496). Although all the experimental facilities for the experimental campaign are made available by ENEA Brasimone Research Center. Views and opinions expressed are, however, those of the author(s) only and do not necessarily reflect those of the European Union or the European Commission. The European Union nor the European Commission can be held responsible for them.*

**satya.saraswat@ing.unipi.it*

1. Introduction

Among the generation IV nuclear reactors, the lead-cooled fast reactor (LFR) has the best chance of becoming the first to attain industrial development [1]. There are also other Generation-IV concepts with recognized relatively high Technology Readiness Level (TRL) level [2]. The Accelerator-driven System (ADS) is a high-stakes initiative in the field of advanced nuclear technology for lead-cooled fast breeder reactors. In this setup, protons with a high-energy spectrum strike the spallation nuclear object (often lead or its eutectic alloy) to generate neutrons through a break-up of a bombarded nucleus process [3]. Research and development activities are also going on in the field of DEMOnstration Power Plant (DEMO) Fusion reactors and other advance generation-IV nuclear reactors [4-16], which also use lead alloy-based fluids (lead-lithium eutectic) and other advance fluids for multiple purposes (coolant, breeder, and neutron multiplier) [17]. Fast neutron spectrum nuclear reactors that use molten lead or lead-bismuth eutectic (LBE) coolant are known as lead-cooled fast reactors. Lead-bismuth eutectic, or LBE, is an alloy composed of lead (at 44.5% by weight) and bismuth (55.5%). Since lead and bismuth have low neutron absorption and relatively low melting temperatures, molten lead or lead-bismuth eutectic may be utilized as the primary coolant [18].

Nuclear reactors that employ molten lead or lead-bismuth eutectic coolant are lead-cooled fast nuclear reactors compared to conventional other fast neutron spectrum nuclear reactors. The lead-bismuth eutectic, or LBE, alloy has 55.5% by weight of bismuth and 44.5% by weight lead. Molten lead or lead-bismuth eutectic can be used as the primary coolant in these types of reactors since lead and bismuth have low neutron absorption and relatively low melting temperatures [19].

Lead-based coolants (LBE and lead-lithium eutectic 99.32 weight percent Pb + 0.68 weight percent Li) have significantly higher boiling points than other liquid metal coolants, like coolants based on sodium (liquid sodium or NaK (Sodium–potassium alloy)). This higher boiling point allows a reactor to be operated at much higher temperatures, frequently without the risk of coolant boiling. Contrary to sodium and NaK, which react violently with water and may ignite in the presence of even a small quantity of air and water, Lead and LBE are only relatively chemically inert in contact with air and water. Despite being essentially transparent to neutrons, lead and bismuth are excellent at blocking gamma radiation due to their thickness and high atomic mass [19]. Rather than the advantages discussed above for utilizing lead-based coolants in fast reactors, there are a few disadvantages with these coolants like (a) Lead and LBE coolants are more corrosive to steel than sodium and NaK eutectic alloys [19], (b) These, together with the very high lead density, places a restriction on the maximum coolant flow velocity within the reactor due to safety considerations and (c) The greater melting temperatures of lead and LBE may also make the coolant solidification a more significant problem when the reactor is operated at lower temperatures.

The fundamental design, safety analysis, and technical advancement of cutting-edge nuclear systems in which heat is transported/removed by heavy liquid metals (HLM) and, most recently, entirely geared to LFRs have been supported since 2000 by ENEA, the Italian National Agency for New Technologies, Energy, and Sustainable Economic Development. ENEA has one of the most extensive European networks of experimental laboratories dedicated to studying HLM thermal-hydraulics, fluid chemical management, corrosion performance for building materials, and material properties in the HLM atmosphere, along with designing modules, equipment, and novel methods, backed by laboratory tests and computational tools. ENEA is also building internationally renowned expertise in fast spectrum core design. Additionally, ENEA, in collaboration with the DICI University of Pisa, initiatives are focused on creating and verifying computational capabilities for HLM operating systems, such as thermal-hydraulic safety analysis by system codes, computational fluid dynamics (CFD) codes addressing their interaction.

Insufficient and unreliable data are all we have on these novel fluids, based on lead alloys like LBE, Lead lithium eutectic (PbLi), and pure lead itself, which is reasonable considering its rarity and is crucial for the safety study of nuclear reactors, which are becoming more popular these days.

The thermo-physical parameters of LBE used by the different nuclear thermal-hydraulic safety analysis system software are mostly derived from chemical handbooks produced in the 1950s and 1960s. [20-22] compiled the first compilation of the key thermo-physical parameters of LBE. One of the most authoritative, recent references on the properties of HLM is presented in [23].

Many of the findings subsequently reprinted without revisions in following manuals [24-29]. Other overview assessments on available information have been found in the literature [30-36]. The resources for the LBE melting point are [20, 21, and 37], which have been generally utilized in various system codes. This information was then repeated in subsequent guides [33] and collections [30, 34-36].

During the examination of relevant literature in the context of the parameter known as the liquid-liquid phase boundary (LBE), as explored in the manuscript under consideration, it has been observed that the melting temperatures of PbBi, as reported in the literature [23-36], fall within the range of 123.5–127.5ºC. Furthermore, the latent heat of melting of PbBi has been found to range from 38.13–38.8 J/g, although the specific methodology employed for these measurements remains undisclosed.

Estimated accuracy is not documented. The temperature range and pressure range are questionable. However, data on the solidification point and latent heat of solidification during the cooling phase are completely missing. However, the specific heat of LBE has a high amount of estimated error, which is about 7%.

The Experimental Engineering Division of the Department of Fusion and Technology for Nuclear Safety, which houses the Nuclear Materials Development Laboratory of the ENEA, has just initiated an experimental campaign to precisely establish the HLM thermal characteristics by employing the DSC equipment that has been installed in that lab. The DSC setup at ENEA served as the site for all the tests conducted for the investigations performed this work.

The primary purpose of the work described in this manuscript is to quantify the lead-bismuth thermal properties for adapting system codes like SIMMER-III to carry out the safety analysis of advanced reactors more accurately. However, the knowledge gained from these measurements will help obtain the lead-lithium properties in the near term as well, after expertise in lead-bismuth, since lead-lithium is very reactive in normal environmental conditions, which is the goal of the experimental campaign run by ENEA, Italy, in collaboration with UNIPI.

This manuscript employs differential scanning calorimetry (DSC) to measure and analyze various thermal properties of lead-bismuth eutectic over a wide temperature range from 25^{o}C to 500^{o}C, ensuring high accuracy and well-defined environmental conditions throughout the experiments. Although attempts were made to extend the investigation to a broader temperature range (up to 1200^{o}C), challenges arose due to rapid evaporation and pressure build-up within the crucible, thermo-couple, and furnace compartment.

Consequently, the experiment setup was disrupted, and reliable data could not be obtained for the higher temperature range of 600^{o}C to 1200^{o}C. This temperature range is well below the boiling point of the LBE, but it was observed during the experiment after temperature increase after 600^{o}C, evaporation of the LBE (can be occurred well below boiling temperature) is dominant and cause buckling and pressure buildup in sample crucible compartment.

We have discussed this situation with our experimental group, performed some literature review, and concluded the reasons for this pressure buildup are as follows:

When LBE is heated at higher temperatures above 600^{o}C, its molecules obtain sufficient kinetic energy to overcome the forces holding them in the liquid, and they escape into the gaseous phase. By doing so, they generate a population of molecules in the vapor phase above the liquid that produces a pressure—the Vapor pressure of the liquid. In the described situation, enough pressure was generated to render the ongoing experiment due to buckling in the local region of the crucible. Since the vapor is contained in an unvented flask and the vapor pressure becomes too high.

Nevertheless, this study serves as a valuable contribution towards understanding and establishing standardized methods and approaches for thermal measurements of reactive liquid metals, such as lead-lithium eutectic, sodium, sodium potassium, molten salt, and others, utilizing DSC. An extensive literature review revealed a scarcity of available evidence, particularly for temperatures exceeding 500^{o}C, about the methodology and procedures for thermal property measurements of such reactive liquid metals. However, it is noteworthy that DSC exhibits a commendable level of

accuracy, consistency, and reproducibility, rendering it a powerful technique capable of comprehensively characterizing the properties of liquid metals, particularly specific-heat properties. This capability holds significant potential for enhancing the predictive capabilities of safety analysis systems and codes predictions in systems employing these technologically advanced fluids as coolants.

2.1 Description of the experimental apparatus

The overall setup of the facility builds at ENEA Brasimone, Italy consists of the following three main components:

1. Main DSC calorimeter (which includes thermo-couples to measure temperature, a furnace to heat the sample and reference crucibles, sensors to detect changes in heat flow, and compartments for sample and reference crucibles where the materials are placed for testing). The main parameters of this component, such as its temperature range and heating rate capabilities, are discussed in Table 1.
2. Protective, cooling, and purge gas systems: These systems are assembled based on the specific requirements of each measurement. Their primary purpose is to control the crucible chambers' temperature, remove any vapors or gases generated during the test using a purge gas, and create an inert environment to avoid any chemical reactions during the measurement. This is particularly important when working with reactive materials that could potentially cause dangerous reactions.
3. Data acquisition and analysis system (which is responsible for recording and analyzing the data generated by the DSC calorimeter, such as the temperature and heat flow changes observed during the measurement).

The complete details of the installed facility, including several of its components (as shown in the original pictures taken during the measurements), and a schematic of the DSC instrument are provided in Figure 1.

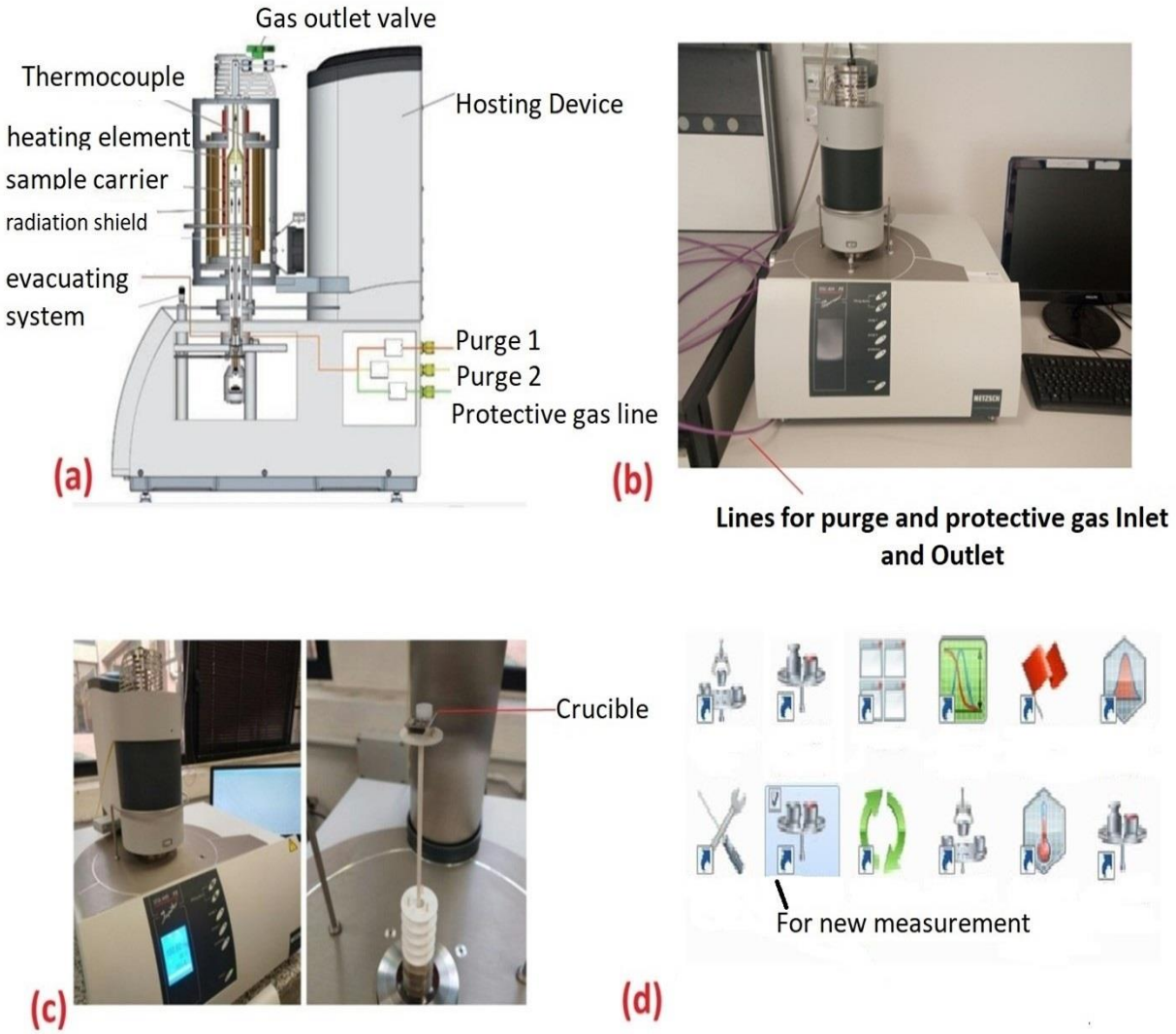

Fig. 1 (a) DSC schematic with various components, (b) Photograph of Complete DSC setup installed at ENEA Brasimone, (c) Photograph of inside the hosting device contains Crucible, heating elements and radiators, (d) NETZSCH-Proteus software installed in windows-based PC with various options, NETZSCH-Proteus

Table 1 DSC equipment Temperature and Heat Flow Measurement design parameters

Accuracy of temperature measurement (%)	Type S: 1.5°C or 0.25% (whichever is greater) Type E: 1.7°C or 0.5% (above 0°C) / 1.0% (below 0°C) (Whichever is greater)
Reproducibility of temperature measurement for metal standards (K)	0.3
Calorimetric sensitivity (µV/mW)	0.4 - 15
DSC baseline linearity (µV) (DSC sample carrier, Thermocouple type S, Platinum furnace)	+/- 2.5
DSC baseline reproducibility (µV) (DSC sample carrier, Thermo-couple type S, Platinum furnace)	0.5
Enthalpy range (J/g)	0 - 30000
Accuracy of enthalpy measurement (%)	+/- 3
Specific heat range (J/kg.K)	10-5000
Accuracy of specific heat measurement (%)	+/- 3
Temperature range for specific heat measurement	-120-1400°C
External power unit	Graphite furnace (max 5000 VA)

3 Results and discussions

3.1 Sample Preparation

Lead-Bismuth (Pb-Bi) sample is prepared in different steps, with various precautions, weighed with very precise (+/-10^{-5} kg accuracy), and in a closed and well-ground labeled compartment. The lead-bismuth (Pb-Bi) sample is prepared in many phases and with numerous precautions (to avoid any impurity) before being weighed with the extreme precision of a scientific weighing machine. The main processes to make a sample are:

1. Cutting the piece from the stored ingot according to our requirements with a very sharp and clean stainless-steel blade,
2. Finishing the surface to avoid any contamination from the surface (removing the upper layer of sample LBE by fine sandpaper); and
3. Hammering to make the sample flat and well-shaped so that it can be heated uniformly in the crucible. Since determining the thermal properties of liquid metals necessitates several sample measurements, which require numerous high-quality crucibles of valuable metals (platinum, molybdenum, etc.), the expense of repeating the tests might rise. Therefore, to reduce the cost of measurements, the chemical treatment of the crucible (so that the contaminated crucible may be used with numerous repeats without costing accuracy) was performed using the chemistry laboratory's resources at ENEA Brasimone. The chemical treatment is done by hydrochloric acid and sulfuric acid at temperatures above 65ºC, and this process takes about 72 hours. The chemical treatment procedure involves the utilization of hydrochloric acid (HCl) and sulfuric acid (H2SO4) at temperatures exceeding 65°C. This process, known as acid treatment, spans approximately 72 hours. During this treatment, the hydrochloric and sulfuric acid are

combined and subjected to a controlled temperature of 65°C or higher. Acids are chosen for their ability to react with the target substance, bringing about desired chemical transformations. The purpose of this procedure is to modify or alter the properties of the material under treatment. By exposing the material to the acidic environment at elevated temperatures, chemical reactions occur, leading to the desired changes in its composition, structure, or other characteristics. Seventy-two hours is necessary to ensure sufficient time for the acids to interact with the material thoroughly. This extended period allows for the completion of the desired chemical reactions, which may involve complex mechanisms or multiple stages. It is important to note that the specific details of this chemical treatment process, such as the nature of the material being treated and the specific concentrations or ratios of the acids used, may vary depending on the intended purpose and desired outcomes. These factors should be carefully considered and optimized based on the specific requirements of the treatment process.

3.2 Procedure adopted for measurements

To begin the new measurement, place the prepared sample material in the sample crucible by elevating the hosting device using manual buttons and then fully closing the hosting machine. At this time, we must additionally monitor and adjust the flow pressures (<=0.6 atm) of the purge and protection gases through the manometers linked to the argon gas cylinder output. We can also check the constant flows during the experiment through the NETZSCH-Proteus software monitoring window.

After completing all manual and hardware processes, the next step (step 2) in measurement is to launch the NETZSCH-Proteus group software, which is installed on Windows operating systems, and then choose the instrument's DSC 404 F1 mode of operation. Start the instrument configuration module following this step to select and validate the required instrument conditions before experiment execution. Following this, we must prepare the header file by defining the identity of the material and sample material weights, describing the crucible (type and material in our case are open Al_2O_3 crucibles), representing the purge and protection gases (argon in our case), and importing the sensitivity calibration and temperature calibration files. Step 3 for the measurement is implementing the temperature program, in which we must set the initial temperature, heating rates, isothermal time, final temperature, and protection temperature range. This step is crucial for the measurement because all subsequent measurements are based on it. The fourth and final step is to analyze the data generated during the test using the NETZSCH-Proteus analyzing module, which allows us to directly determine the melting point, latent heat of vaporization, and specific heat capacity (though specific heat capacity measurements require a slightly different procedure and at least two samples + correction runs under the same conditions and heating rate).

All these steps discussed above used in different tests are presented in Tables 2 to 3

Table 2 (a) Step 2 Header file creation

Sample identity:	Pb-Bi
Sample name:	Lead-Bismuth Eutectic
Sample Mass:	292.8 mg
Crucible:	$Al2O_3$, 85 µl, open
Crucible Mass:	132.9 mg
Reference name:	$Al2O_3$
Reference Mass:	0 mg (empty crucible)
Reference Crucible Mass:	132.9 mg
Material:	$Al2O_3$
Sample determination mode:	Manual

Table 2 (b) other details

Instrument:	NETZSCH DSC 404F3 DSC404F3A-0272-M
Project and funding agency	Eurofusion
Filename:	satya_May24_run7_PBBI.ngb-sd9
Method used:	DSC new measurement
Laboratory:	ENEA
Operator:	Satya Prakash Saraswat
Measurement Type:	Sample
Temp.Calib. file used	TCALZERO.TMX
Crucible:	Al_2O_3 85 µl, open
Remark:	Argon gas environment
Furnace:	SiC S
Sample carrier:	DSC Cp S
Measurement End:	Normal end
Furnace TC:	S type
Sample TC:	S type

Table 3. Temperature program for different measurements with heating rate (5-20 K/min)

Number	**Mode**	**Temperature °C**	**HR (Heating Rate) K/min**	**Acq.Rate pts/min**	**Duration hh:mm**	**Purge Gas (PG) line 2 Argon flow rate**	**Purge Gas (PG) line 1 Argon flow rate:**
0	Start	25-40.0				20.0	50.0
1	Dynamic	300.0	5-20	100.00	00:16-01:00	20.0	50.0
2	Isothermal	300.0		300.00	00:01	20.0	50.0

Number	Mode	Temperature °C	HR (Heating Rate) K/min	Acq.Rate pts/min	Duration hh:mm	Purge Gas (PG) line 2 Argon flow rate	Purge Gas (PG) line 1 Argon flow rate:
3	Emergency	310.0				20.0	50.0
4	Final stand-by heating	20.0	40		00:04	20.0	50.0
5	Final stand-by isothermal	20.0			02:00	20.0	50.0

3.3 Crucible requirements and selection:

The alumina crucible was chosen for all the experimental tests in the current study. The reasons for the selection of this material for the crucible are justified in the text below.

In DSC experiments, significant performance is guaranteed if you use the correct crucible. In addition to influencing the accuracy of the measured data, the crucible employed may also affect crucial properties of the Thermogravimetric Analysis (TGA) and DSC response. There are many benefits to using alumina crucibles in the Pb-Bi eutectic thermal measurements:

1. These crucibles are available in large quantities, increasing the sensitivity of DSC and enhancing experimental precision. The clarification of this point is provided below this paragraph.
2. The high purity of the material in these crucibles eliminates sample-crucible interaction.
3. The crucibles' high form stability is ensured.
4. Flatness ensures perfect thermal contact, which is essential for these experiments.
5. These crucibles can be reused after chemical treatment.

To determine the properties of a material using Differential Scanning Calorimetry (DSC), it is necessary to conduct a series of experiments with varying system parameter values. Even repeated experiments with the same system parameters are required to eliminate any system error in the measurement. These parameters include heating rates, purge gas flow rates, and other relevant factors. Consequently, many identical crucibles are required to facilitate the repetition of these experiments (since after one investigation with a crucible, it needs to be chemically treated, which involves a lot of time)

To ensure reliable and accurate results, it is crucial to repeat the experiments under different conditions. By systematically varying the system parameters, this approach allows for a comprehensive understanding of the material's response to different conditions, aiding in identifying and characterizing its properties.

To perform these repeated experiments, a higher number of identical crucibles is necessary. Crucibles are the sample holders that contain the material being analyzed in the DSC instrument. Using identical crucibles for each experiment ensures consistency and eliminates the potential for systematic errors arising from variations in the crucible properties themselves.

By increasing the number of crucibles available, we can conduct more repeated experiments, encompassing a more comprehensive range of system parameter values. This increased experimental diversity leads to a more robust and statistically significant dataset, enhancing the accuracy and reliability of the obtained results.
Therefore, having a higher number of identical crucibles is essential in improving the accuracy of DSC experiments, as it enables the repetition of experiments with different system parameter values, facilitating a comprehensive exploration of the material's properties under varied conditions.

3.4 Calibration required for measurements

The baseline calibration is selected as the primary DSC test whereby an empty reference crucible is heated throughout a wide range of temperatures. The resulting profile is being used to compensate for differences in crucible heat flow across the sample and reference crucibles. Usually, this test is called a "correction test."

A typical DSC test is used to calibrate the temperature at which a reference material is heated through a recognized transition (e.g., the indium melting point in our case of Pb-Bi). The reported phase transition temperature is compared to its reported value to calculate a calibration factor. Using at least two calibration standards that span the temperature range of interest is advised.

In this paper, the calibration for melting and solidification was conducted using pure indium as the reference material with a purity of 99.999 percent. The scientific community widely accepts using pure metal calibration [37-38]. However, it is essential to acknowledge that alternative calibration methods or reference materials may sometimes be employed. Certified reference materials (CRM) developed explicitly for alloys, or intermetallic compounds can be viable alternatives. The selection of the calibration approach hinges upon the specific requirements, available resources, and desired analysis accuracy.
Characterizing a sample metal material with a pure metal calibration reference is commonplace because it facilitates accurate and standardized analysis of the sample's composition and properties. The following factors shed light on the rationale behind this approach:

1. Pure metals function as calibration standards, providing a well-defined and known composition against which the sample can be compared. These standards are meticulously characterized and certified by standardized organizations or laboratories, ensuring their accuracy and reliability. By comparing the sample's response to the known properties of the pure metal reference, valuable insights regarding the sample's composition, impurity levels, and other pertinent characteristics can be derived. Prior studies have also employed indium as a calibration reference to determine the properties of LBE [37-38]. Indium's closer melting point value to LBE facilitates the analysis of DSC.
2. Metal alloys often possess intricate compositions of multiple elements in varying proportions. By characterizing a sample using a pure metal reference, scientists can accurately determine the presence and concentration of each component. This

information is crucial for quality control, material selection, and identifying impurities or variations that may impact the material's properties.

3. Pure metals typically exhibit well-defined physical and chemical properties, encompassing parameters like melting point, electrical conductivity, and mechanical strength. Comparing these properties with those of the sample metal material aids in assessing its quality, consistency, and performance. Using pure metal calibration references, we can establish a benchmark for evaluating desired properties while identifying deviations or improvements within the sample.
4. Standardization and Reproducibility: Pure metal calibration references contribute to standardization and reproducibility across diverse laboratories and research facilities. This approach enables researchers to compare and validate their results using shared reference material, ensuring consistency and reliability in their findings. Such practices are significant in fields like metallurgy, where accurate and repeatable analyses are essential for broad industrial applications.

A traditional DSC test procedure is also used for heat flow calibration, wherein the reference metal is heated through a well-characterized changeover (e.g., indium melting point in our case of Pb-Bi). The heat flow that facilitates the transition is evaluated to calculate a calibration factor by comparing it to the theoretical values.

A DSC investigation using a recognized standard, such as platinum, is used to calibrate heat capacity [39].

By using platinum as a reference material in DSC experiments, we can obtain precise and reliable measurements of the heat capacity of LBE [39]. The known heat capacity and favorable thermal properties of platinum contribute to accurate calibration and referencing, leading to a more precise determination of heat flow and heat capacity in the target material. Platinum is often used as a reference material to determine the heat capacity of Lead-Bismuth Eutectic (LBE) using the Differential Scanning Calorimetry (DSC) technique due to several reasons:

1. Platinum has a relatively high melting point and is thermally stable at the temperatures typically encountered in DSC experiments. This characteristic makes it compatible with the temperature range at which LBE undergoes phase transitions or exhibits thermal effects that are of interest for heat capacity measurements.
2. The heat capacity of platinum has been extensively studied and well-documented. Its heat capacity is known over a wide temperature range, allowing accurate calibration, and referencing in DSC experiments. The heat flow and heat capacity of LBE can be determined by comparing its thermal behavior to platinum.
3. Platinum has relatively high thermal conductivity, ensuring efficient heat transfer within the DSC sample cell. This property helps achieve better temperature equilibration and accurate heat flow measurements during phase transitions or thermal events in LBE.

When employing an intrinsic heating rate, a single calibration value is employed, and it must be found around the midpoint of the target temperatures in the range and near the transition of interest (when making isothermal measurements). Alternatively, numerous calibrations may be averaged and utilized to cover the temperature range of interest. The best results are achieved when 25mg (nominal) of sapphire is used under identical circumstances as in the following

sample tests. Prolonged durations (>2 minutes) give the highest accuracy for heat capacity assessments since they allow for the most heat transmission out via the sample.

To correctly estimate the correction factor, the test circumstances (e.g., pan type, purge gas, heating rate, modulation amplitude, and period) in all calibrations have been considered like those used in successive sample assessments since calibration is strongly reliant on these factors. Figure 2 shows the sensitivity calibration which has been obtained by the standard procedure discussed above and has been utilized for the tests performed in the current study.

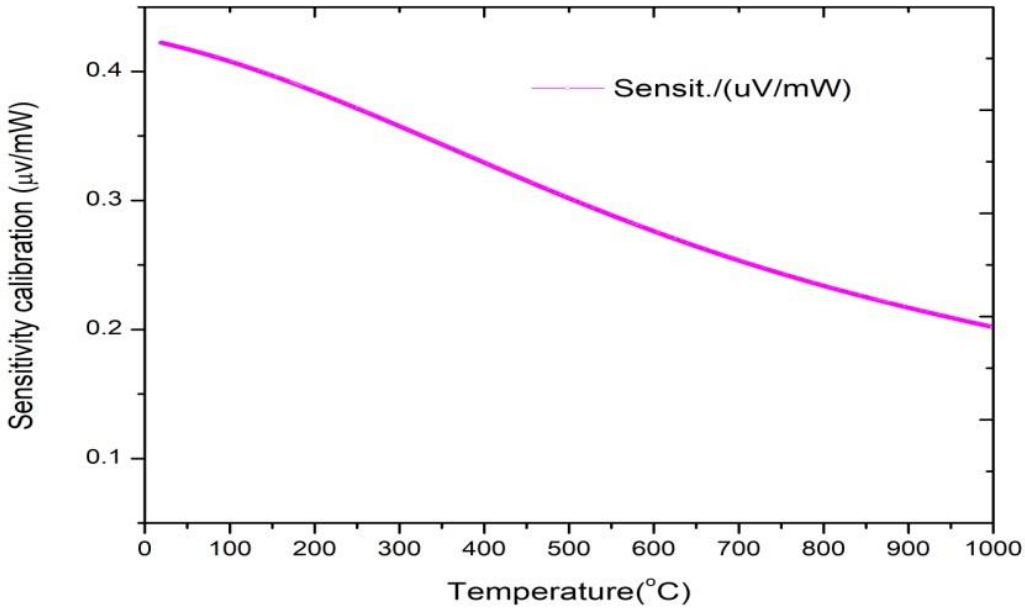

Fig. 2 Sensitivity calibration obtained for alumina crucible and for purge and protection argon gas flow 20 ml/min and 50 ml/min respectively

4. Experimental tests

4.1 Tests executed and their objectives:

Several tests have been performed to accurately predict the Pb-Bi thermal properties but only twelve most relevant and successful tests have been discussed here. These twelve experiments were successfully completed to assess the thermal characteristics of Pb-Bi. The first test is the corrective test, performed with both empty and identical crucibles. The purpose of this test is to determine any inconsistency between the two crucibles heating and the measurement of DSC output and then use that information to calculate the correction factor for precisely measuring sample attributes.

The next four tests are convenient novel sample tests for measuring melting temperature and latent heat of melting for different values of heating rates (5 K/min, 10 K/min, 15 K/min and 20 K/min), while the sixth and seventh tests are for determining the point of solidification temperature and latent heat of solidification. Tests from 8 to 11 are used for determining the

specific heat capacity of LBE (up to 500^{o}C). The final test (12th test), which is the most ambitious, is performed for the measurement of specific heat capacity at higher temperature ranges (500^{o}C to 1200^{o}C). Still, this test is not entirely successful due to the rupture of the sample crucible base platform during the test. Despite the technically and characteristically based analysis of this specific test providing very useful information for potential tests at higher temperature ranges (specifically for lead-based alloys), the details of which are provided below.

To verify the accuracy and consistency of the experimental findings from various experiments performed for each standard LBE sample. The temperature and heat correction factors are computed for a broad range of heat and temperatures. The calibration files for temperature and heat sensitivity calibration are then prepared based on these correction factors, and they are used for the sample plus correction type of measurement for additional precision. The procedure for performing the correction experiment on DSC equipment has already been discussed in the previous section. The same sample has been tested four times for extra accuracy in determining the thermal properties (the melting point, latent heat of melting, solidification point, and latent heat of solidification). The sample specification, the environmental conditions during the execution of the experiment, and the detail of the experimental setup are described in Tables 2 and 3.

DSC output is typically reported in units of mW/mg. This unit represents the heat flow or power per unit mass of the sample being analyzed.

In a DSC experiment, the instrument measures the heat flow or power differential between the sample and reference material as a function of temperature or time. The mass of the sample often normalizes this heat flow to account for variations in sample size. It facilitates comparisons between samples, so mW/mg provides a standardized measure of the heat flow per unit mass. This allows for meaningful comparisons of thermal behavior or energy changes within different samples, considering their varying masses.

The mW/mg output in DSC analysis provides information about the specific heat capacity, enthalpy changes, phase transitions, or thermal effects of the sample material on a per-unit-mass basis. It assists in understanding the thermodynamic properties and behavior of the sample under various temperature conditions.

Figure 3 shows the correction type of experiment with an empty reference and a sample crucible. The graph has been plotted in the NETZSCH-Proteus software using the analyzing tab. In the graph, the red line shows the temperature program (25^{o}C to 500^{o}C) with segments for isotherm for protection. A blue line displays the DSC output (µV/mg) for the entire temperature range. The magenta and sky-blue lines show the protection and the purge gas (argon) profiles during the experiment (constant flow of 20 and 50 ml/min, respectively). This correction graph, along with the temperature and sensitivity calibration files, has been imported and utilized for all experimental tests for the thermal property measurement of LBE for accuracy purposes.

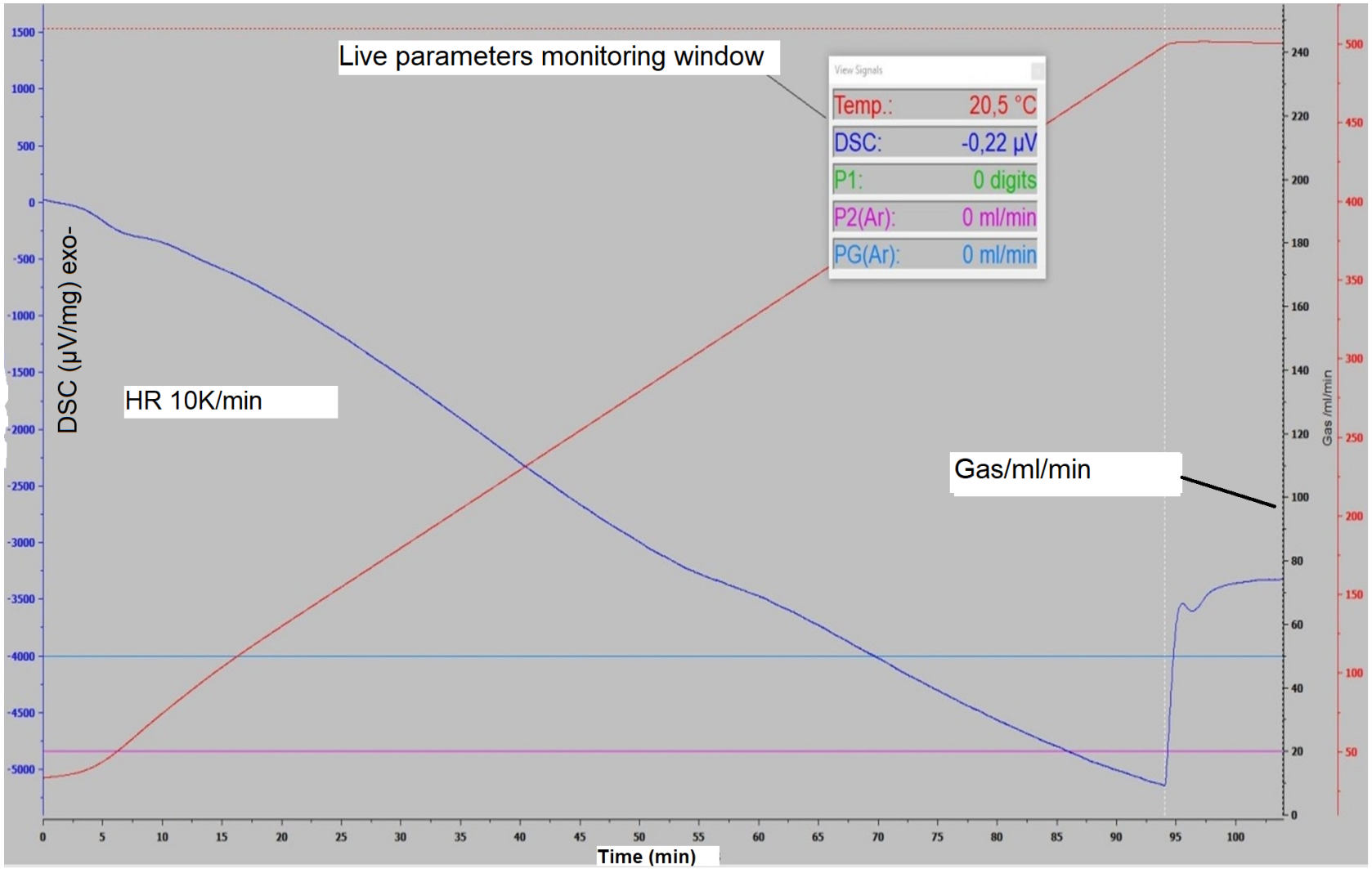

Fig. 3 Correction type of experiment with empty reference and sample crucible.

4.2 Tests 2-5: These tests were carried out at ENEA, Brasimone, from May 24 to May 25, 2022, to correctly measure the melting temperature and the latent heat of melting within the uncertainty of the measurements and the chosen technique. The varied heating rates (5 K/min, 10 K/min, 15 K/min, and 20 K/min for tests 1 to 4, accordingly) are considered for different tests since the heating rates significantly impact measured values. We have determined the melting point and latent heat of melting for these four heating rates. The same LBE sample and alumina crucible are used for these tests. All other parameters during these tests are held constant and explained in earlier sections (Tables 1, 2, and 3). The purge gas (Argon) and protection argon gas flows were maintained constant (20 ml/min and 50 ml/min, respectively), and the calibration files were carefully created for these gas flow values. An average strategy was utilized to establish the values of these parameters accurately after the successful execution of these experimental tests. More clearly, Multiple tests are performed to determine a parameter, and the average value is obtained by averaging the test values. This approach improves accuracy by considering variations and uncertainties, providing a more reliable parameter estimate. Figure 4 depicts a sample + correction type verification test experiment with LBE in the sample crucible. It was only to test the experimental equipment for appropriate operation. The output profile of the DSC (recalibrated to mW/mg) is measured because of the time-based furnace power increment variation [40-41]. The arrow with the word "exo." illustrates the direction of an exothermic reaction with DSC output, which implies that when the reaction is exothermic with continual heating, the DSC output is in the negative direction (in particular, in the case of LBE). The temperature profile during continual heating is depicted in Fig. 5, allowing us to confirm that the furnace is generating consistent heat throughout time. Although during the phase change of the material (solid to liquid), the DSC output's direction reverses, indicating that the sample has observed heat at a higher rate than the heat rate provided by the furnace. Figures 5 to 8 show the DSC profiles, the melting points (124.3^{o}C for heating rate 5 K/min, 124.4^{o}C for heating rate 10 K/min, 124.4^{o}C for heating rate 15 K/min, and 124.8^{o}C for heating rate 20 K/min) and the latent heats of melting observed are (37.93 J/g for heating rate 5 K/min, 37.89 J/g for heating rate 10 K/min, 37.64 J/g for heating rate 15 K/min, and 41.81 J/g for heating rate 20 K/min). In database mentioned in “OECD/NEA HLM Handbook” [23] by different studies (with unknown technique and unknown system conditions) the LBE normal melting temperature ranges in between (123.5^{o}C-127.5^{o}C) in compared to the melting point measured by our experiment campaign is in the range of (124.3^{o}C-124.8^{o}C). Our results contribute to the existing database by providing superior knowledge of the experimental conditions, enhancing the overall understanding of the subject matter.

From Figures 5-8, it has been observed that for higher heating rates, the values of the parameters have a very high deviation compared to those of lower heating rates. This may be due to the high thermal stress and buckling of the crucibles for high-temperature rates.

Therefore, heating rates higher than 15 K/min are not suggested, and the measured values for heating rate in Test 5 are not included in evaluating the melting points and the latent heats of

melting. Figure 9 shows the summary of tests 2 to 5 in one plot, the range of melting points, and the latent heats of melting for a clear picture for the audience.

The average of tests 2 to 4, excluding test 5, gives the value of the average melting point of 124.367^{o}C and the average latent heat of melting of 37.82 J/g. We are unable to remark on the uncertainty and inaccuracies in the results of tests 2 and 4 from Figure 4 to Figure 9. In the last portion of this publication, the analysis of findings' degree of uncertainties in parameters is summarized. This might be reformulated indicating that uncertainties are estimated in Section 5.

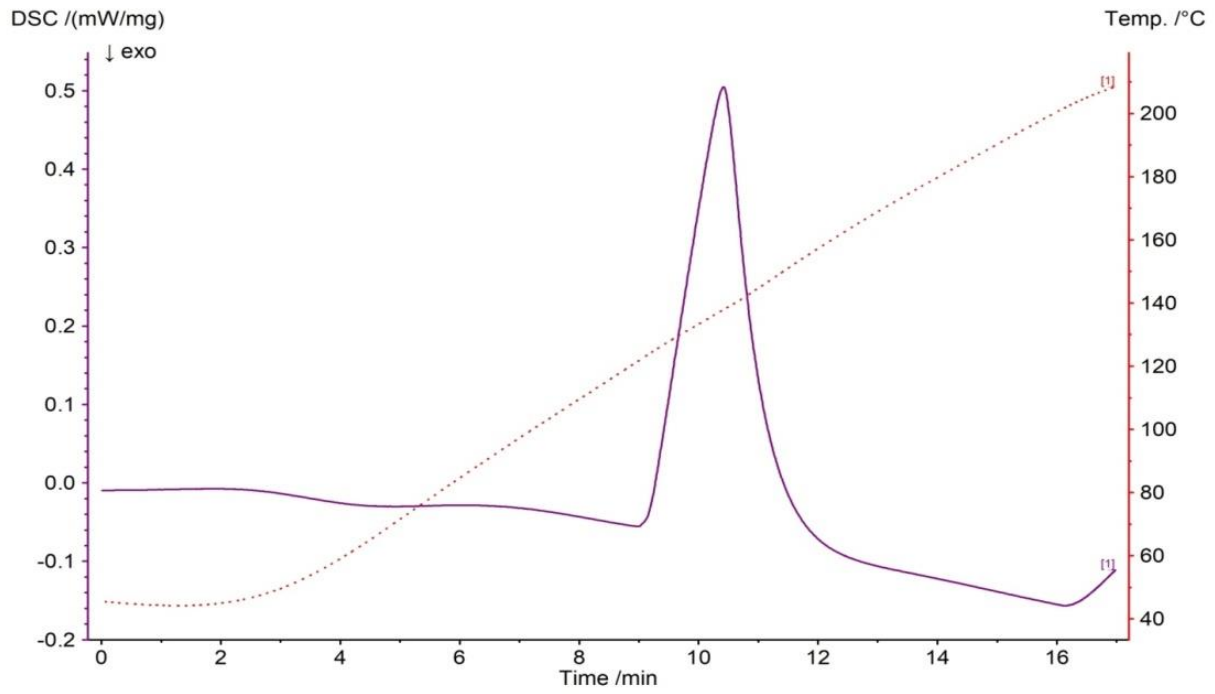

Fig. 4 A general Sample + correction measurement test 1 with imported calibration files for temperature and sensitivity

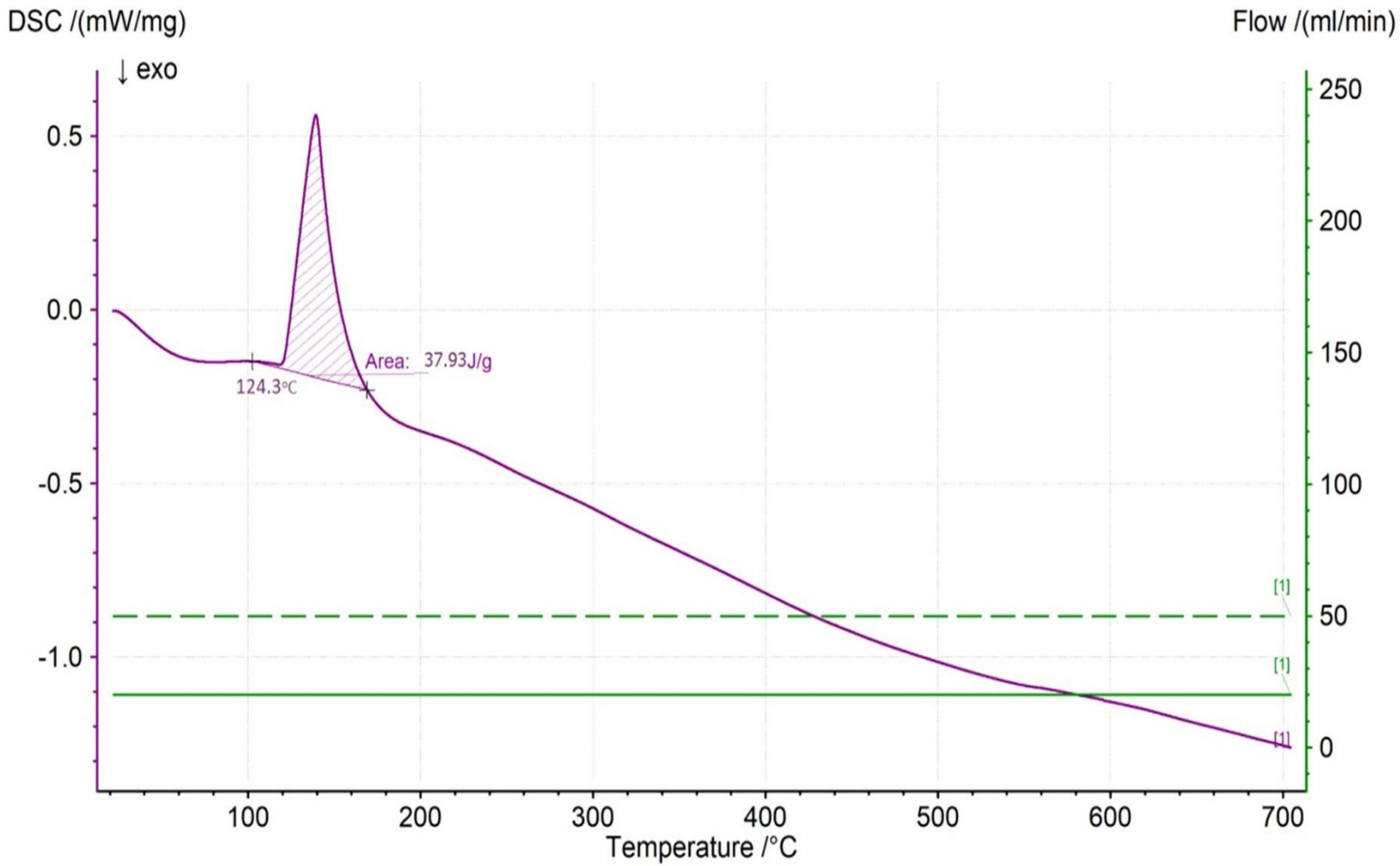

Fig. 5 DSC experiment test 2, measurement of melting point temperature and latent heat of melting with a heating rate of 5 K/min; Argon gas environment and other details are given in figure footer.

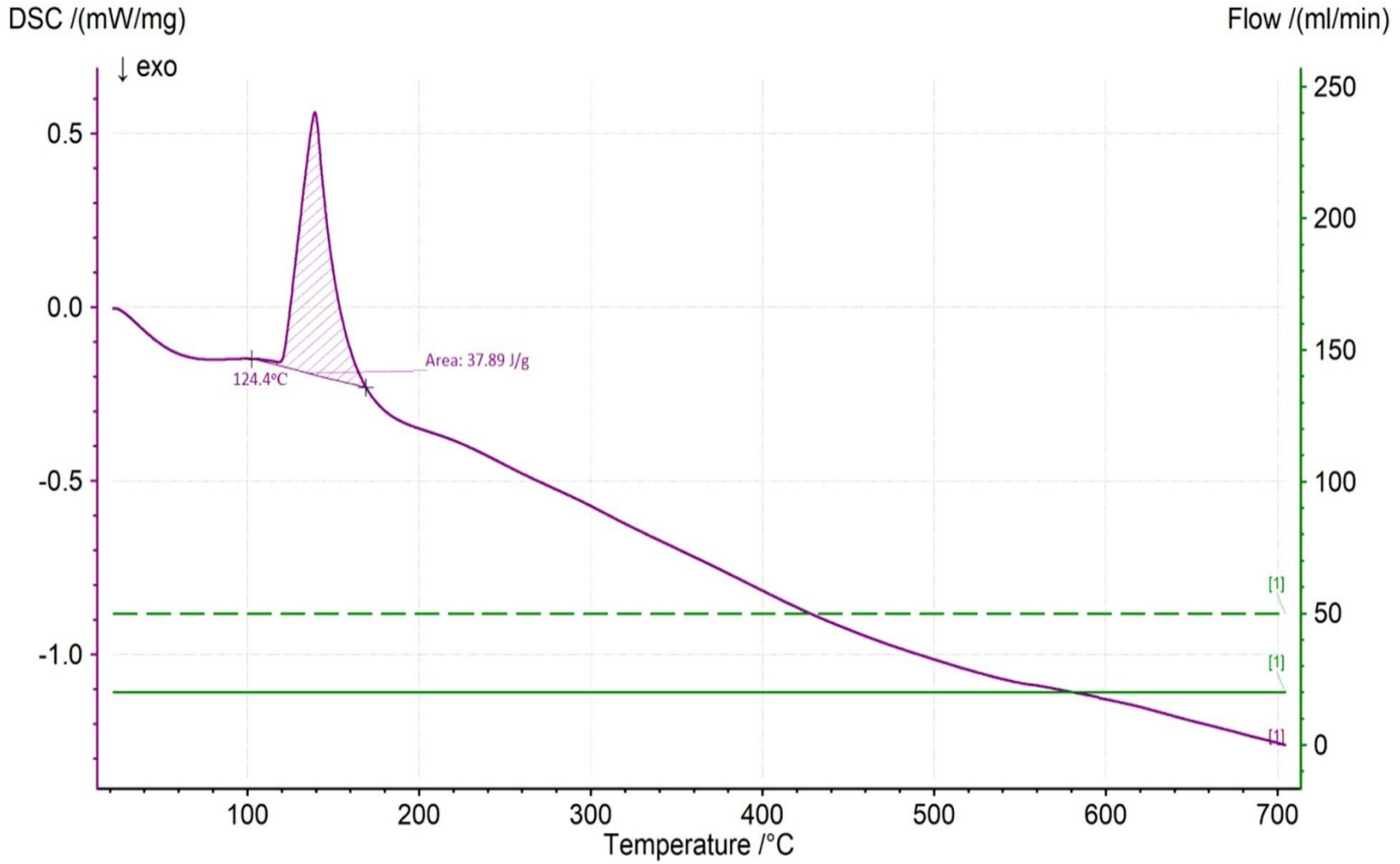

Fig. 6 DSC experiment test 3, measurement of melting point temperature and latent heat of melting with a heating rate of 10 K/min; Argon gas environment and other details are given in figure footer

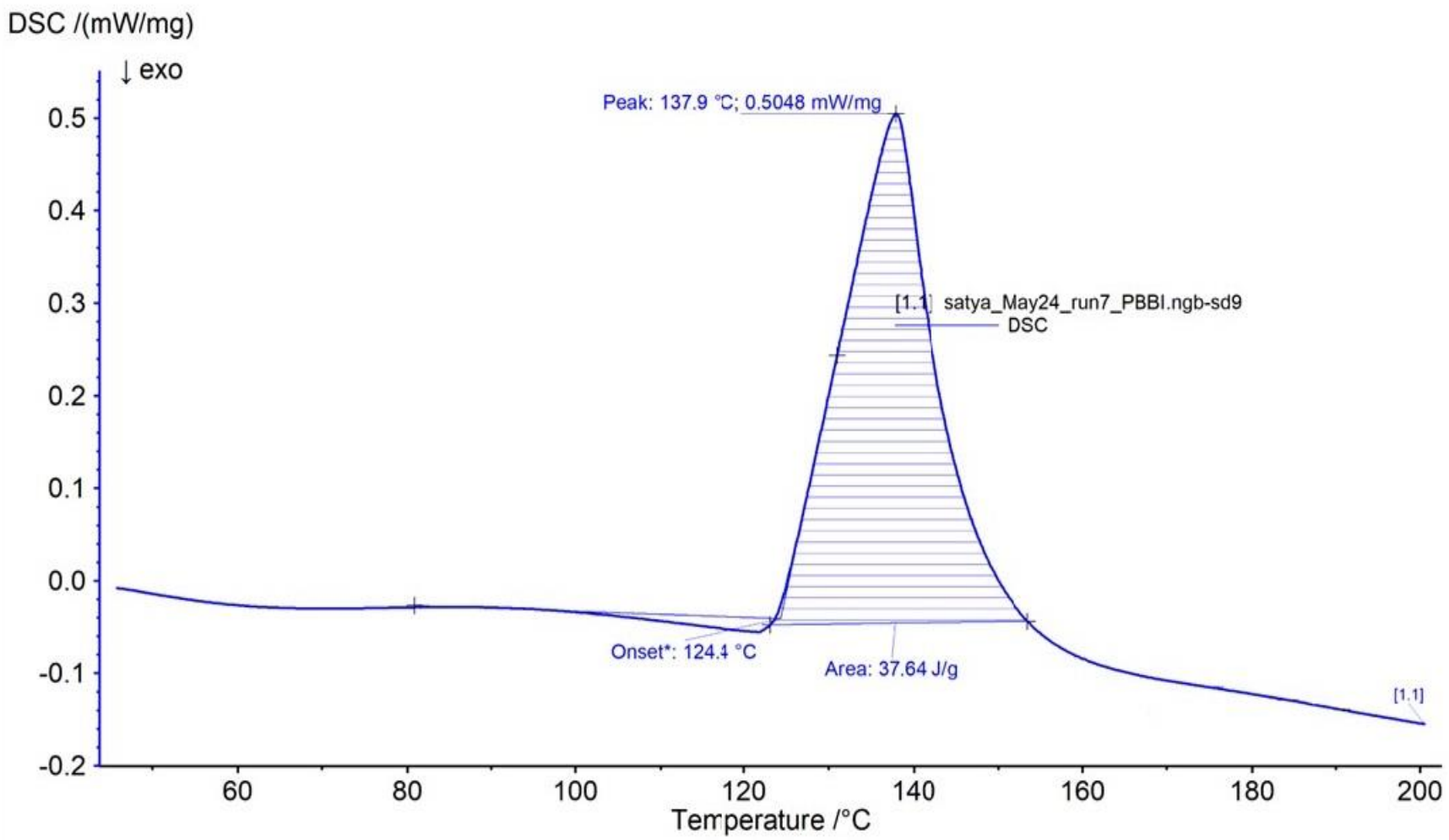

Fig. 7 DSC experiment test 4, measurement of melting point temperature and latent heat of melting with a heating rate of 15 K/min; Argon gas environment and other details are given in figure footer.

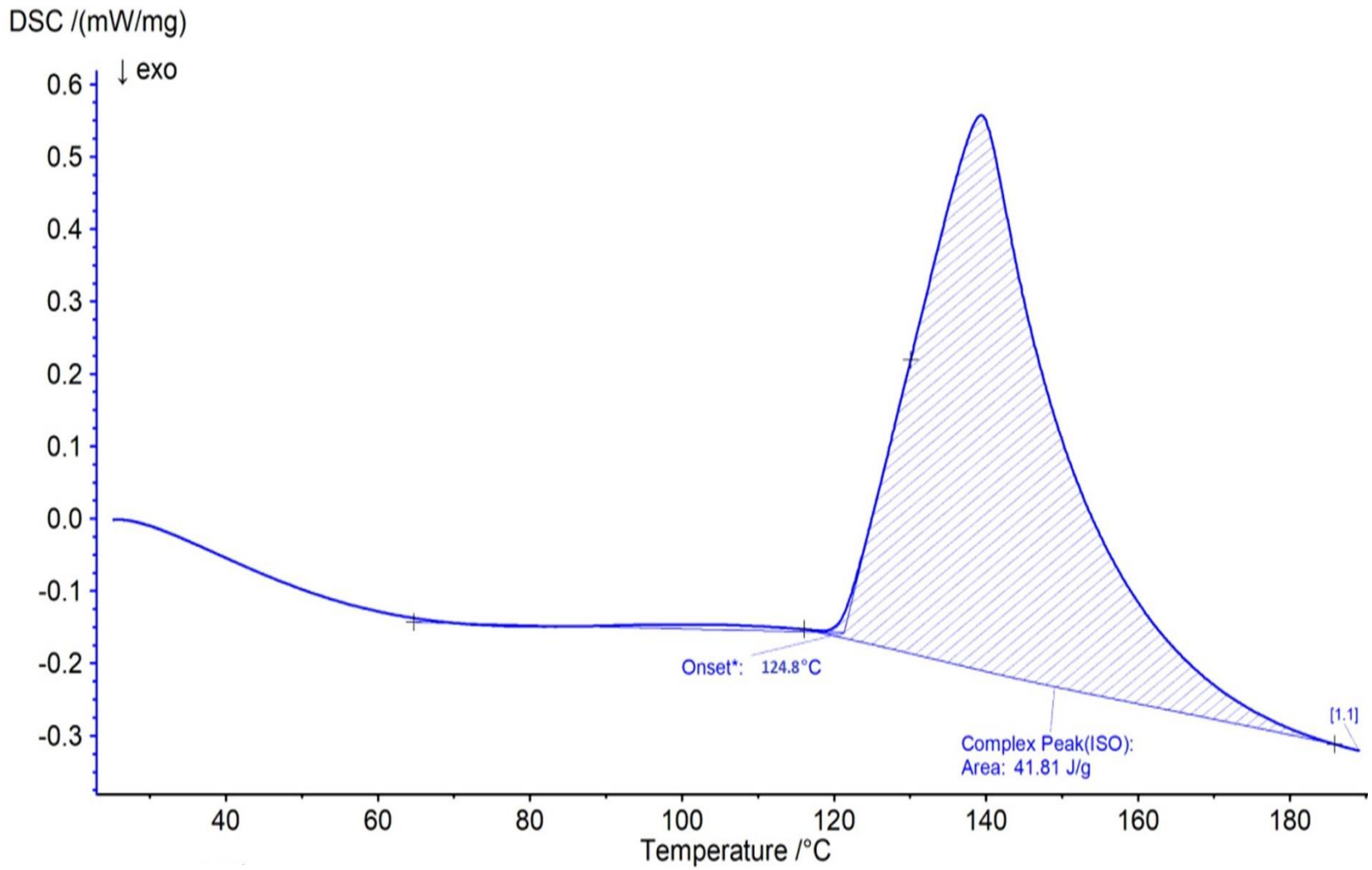

Fig. 8 DSC experiment test 5, measurement of melting point temperature and latent heat of melting with a heating rate of 20 K/min; Argon gas environment and other details are given in figure footer.

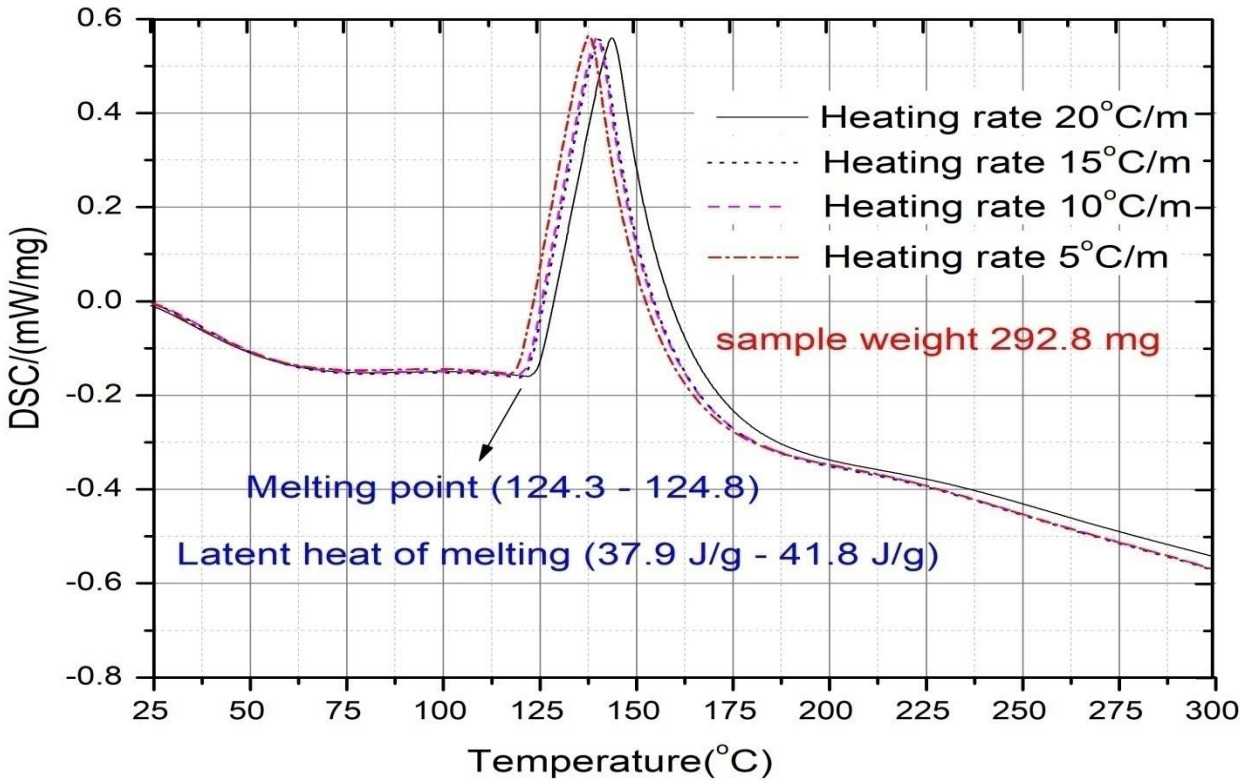

Fig. 9 Summary of DSC experiment tests 2-5

4.3 Tests 6 and 7: These tests were carried out at ENEA, Brasimone, on May 24, 2022, to correctly measure the solidification temperature and the latent heat of solidification within the uncertainty of the measurements and the chosen technique. The varied heating rates (5 K/min, 10 K/min for tests 6 to 7 accordingly) are considered for different tests since the heating rates significantly impact measured values. We have determined the melting point and latent heat of solidification for these two heating rates. The same LBE sample and alumina crucible are used for these tests.

The details of the components and parameters during tests 6 and 7 are provided in the footer of Figures 10 and 11. Figure 10 shows the DSC output (mW/mg) profile and temperature program with heating rate 10 K/min, while Figure 11 shows the DSC output (mW/mg) profile and temperature program with heating rate 5 K/min.

The temperature profile during continual heating and cooling can be observed in Fig. 10 and 11, allowing us to confirm that the furnace is generating consistent heat throughout time. Although during the phase change of the material (solid to liquid and liquid to solid), the DSC output's direction reverses, indicating that the sample has experienced heat at a higher/lower rate than the heat rate provided by the furnace. Figures 10 and 11 show the DSC profiles, the solidification points (140.5ºC for cooling rate 10 K/min and 140.2ºC for cooling rate 5 K/min) and the latent

heats of solidification observed are (36.5 J/g for cooling rate 10 K/min, 36.80 J/g for cooling rate 5 K/min).

Here from Figures 10 and 11 we cannot comment on the uncertainty and errors in the values of test 6 and 7. The analysis of uncertainty in the results and their summary is presented in the last section of this manuscript. This might be reformulated indicating that uncertainties are estimated in Section 5.

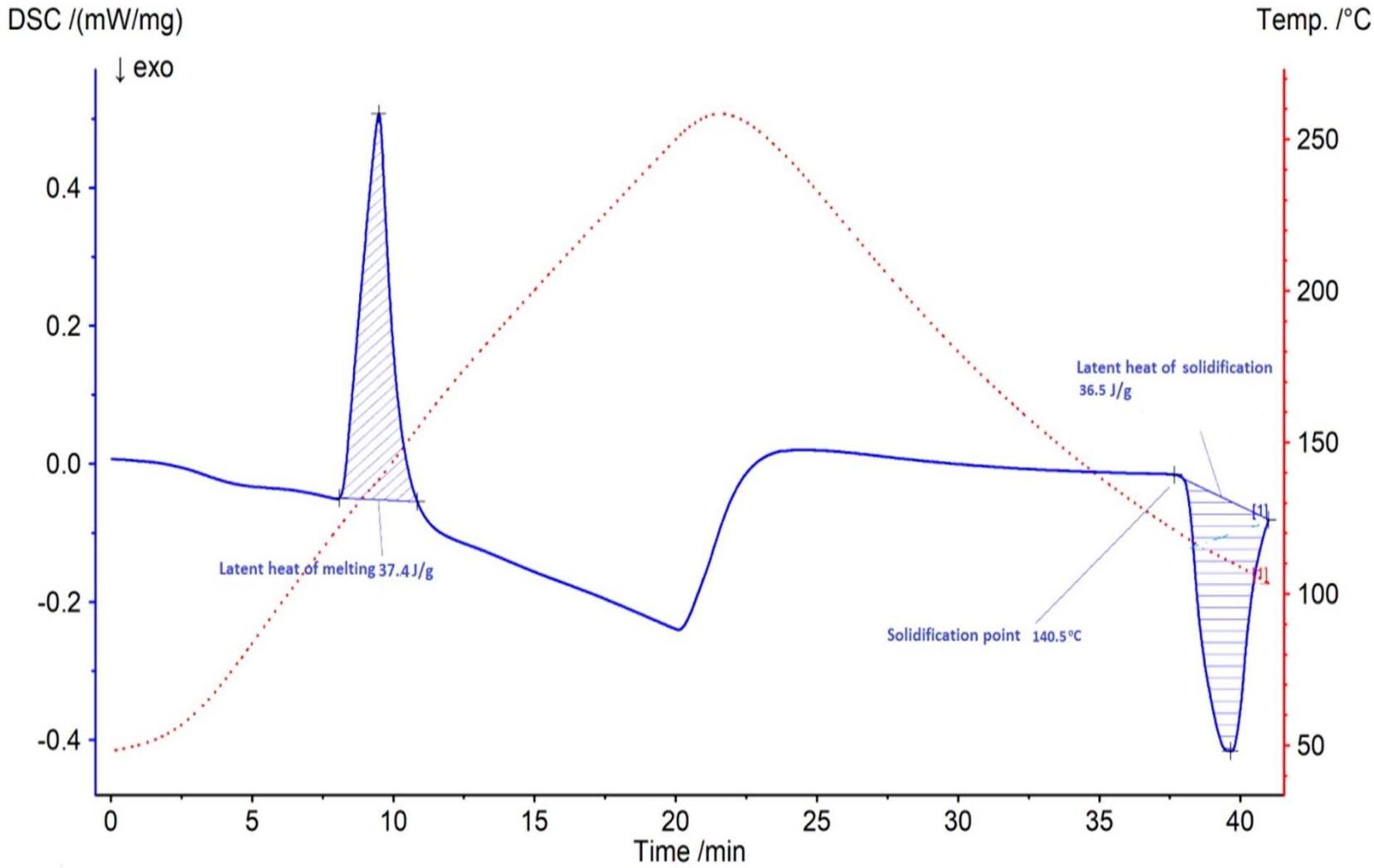

Fig. 10 DSC experiment test 6, measurement of solidification point temperature and latent heat of solidification with a cooling rate of 10 K/min; Argon gas environment and other details are given in figure footer.

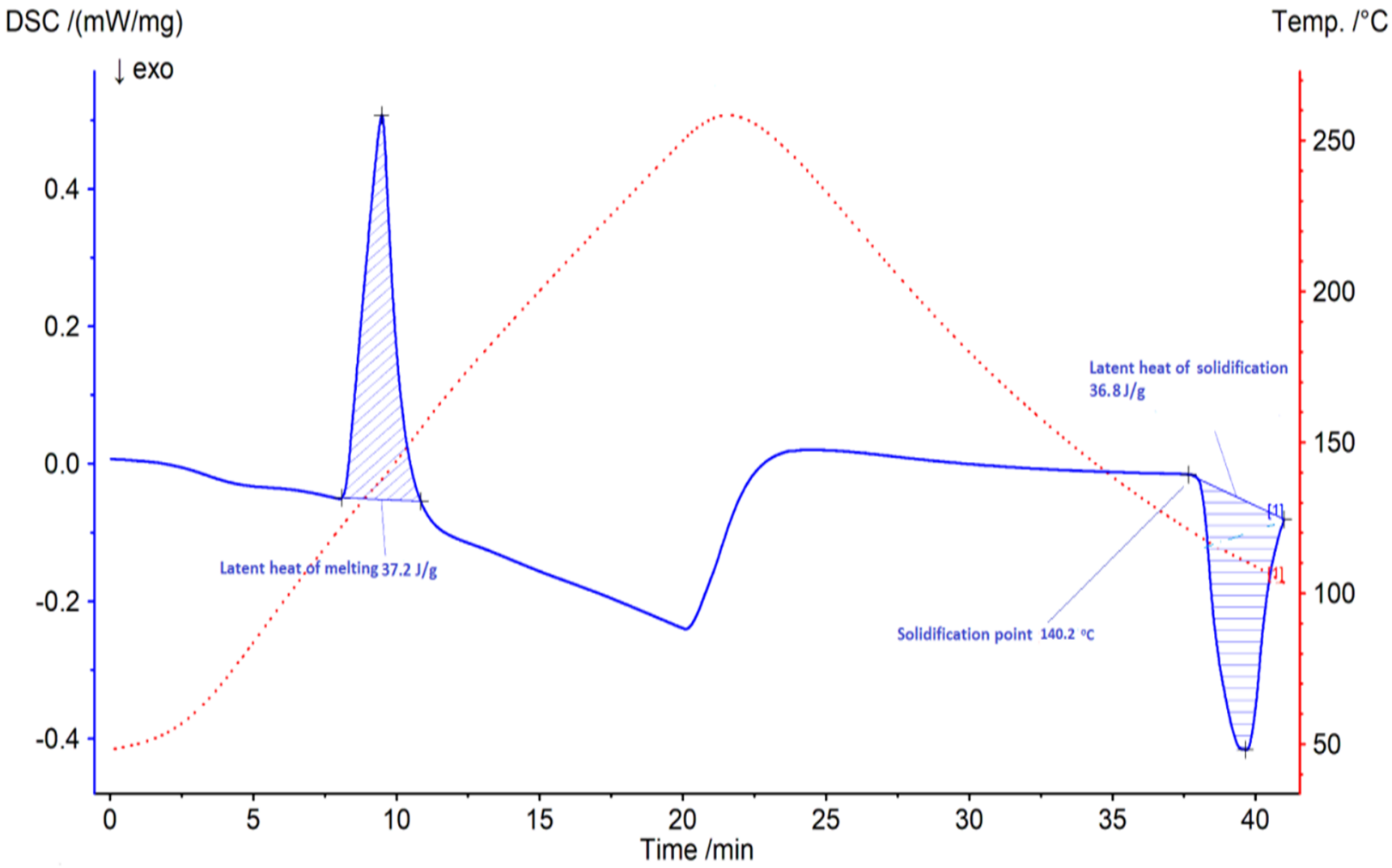

Fig. 11 DSC experiment test 7, measurement of solidification point temperature and latent heat of solidification with a cooling rate of 5 K/min; Argon gas environment and other details are given in figure footer

4.4 Measurement of the specific heat (Tests 8 to 11)

Experimental tests 8 to 11 are dedicated to the measurement of specific heat using DSC. These tests were conducted at ENEA, Brasimone, on May 25, 2022. It takes a little more effort to measure specific heat capacity using DSC since it necessitates at least two samples plus correction type operations for a single measurement using a calibration file for the heat capacity from reference materials (in our case we have utilized the Platinum for the latent heat and heat capacity calibration). All other circumstances, such as gas flow rates, heating rates, temperature profiles, and purge gas pressure, must be kept equal throughout the two independent samples plus correction kinds of experiments to determine the good accuracy in measurement. Table 4 provides details of components and parameters utilized during specific heat measurements. The details of sample and reference crucibles are provided in Table 5. Table 6 shows the temperature program during the tests 8 to 11. Table 7 shows average experimental tests data (8 to 11) temperature, DSC output and specific heats with temperature range (20.0^{o}C to 500^{o}C)

The outcomes of the experimental tests 8 to 11 are reported in Figures 12 and 13. Figure 12 displays the findings of Tests 8 and 9 with the same heating rate of 5 k/min, whereas Figure 13 displays the results of Tests 10 and 11, with the same heating rate of 10 k/min. Although this experiment uses a temperature variation program, the DSC primarily monitors the heating rate. The specific heat capacity is determined via the computer's licensed NETZSCH DSC Proteus application package. The specific heat variance for a uniform temperature increases from 30°C to 500°C is shown in Figures 12 and 13. Figure 14 compares the average LBE specific heat capacity as obtained experimentally with data from published sources.

It is important to note that all the obtained results in our analysis have been meticulously compared with the data provided by various researchers mentioned in the OECD/NEA HLM Handbook [23]. This handbook serves as a comprehensive compilation of research findings contributed by different investigators in the field. The rigorous comparison against these established references ensures the reliability and validity of our study's outcomes.

Here in this section only the measured values are presented in Figures 12 and 13, while the average values of the heat capacity are presented in Table 7. We are unable to remark on the uncertainty and inaccuracies in the results of tests 8 to 11 from Figures 12 and 13. In the last portion of this publication, the analysis of findings' degree of uncertainties in parameters is summarized.

Table 4 Details of components and parameters during specific heat measurement

Instrument:	NETZSCH DSC 404F3 DSC404F3A-0272-M
Date/Time:	25/05/2022 09:32:20 (UTC+1)
End Date/Time:	25/05/2022 10:19:21 (UTC+1)
Laboratory:	ENEA
Measurement Type:	sample with correction

Temperature Calibration	25-05-2022 16:41
Sensitivity:	25-05-2022 11:07
Crucible:	Al_2O_3 85 µl, open
Furnace:	SiC, S
Sample carrier:	DSC Cp S
Measurement End:	Normal end
Furnace TC:	S
Sample TC:	S
Number of repetitions	2

Table 5 Sample crucible parameters details

Sample identity:	Sample + correction
Sample name:	PbBi
Sample Mass:	63.5 mg
Crucible:	Al_2O_3 85 µl, open
Crucible Mass:	132.9 mg
Reference name:	PbBi
Reference Mass:	0 mg
Reference Crucible Mass:	132.9 mg
Material:	Al
Sample determination mode:	Manual

Table 6 Temperature Programme for specific heat measurement

Num.	**Mode**	**Temp. °C**	**HR K/min**	**Acq.Rate pts/min**	**Duration hh:mm**	**STC**	**P2: Ar**	**PG: Ar**
0	Start	40				1	20.0	50.0
1	Dynamic	500	5/10	100	00:46	1	20.0	50.0
2	Isothermal	500		300	00:01	1	20.0	50.0
3	Emergency	510					20.0	50.0
4	Final stand-by heating	20	40.000		00:12	1	20.0	50.0
5	Final stand-by isothermal	20			02:00	1	20.0	50.0

Table 7 average experimental tests data (8 to 11) temperature, DSC output and specific heats with temperature range (20.0ºC to 500ºC)

Temperature /°C	**DSC/(mW/mg)**	**Cp /(J/(g*K))**	**Temperature /°C**	**DSC /(mW/mg)**	**Cp /(J/(g.K))**
21	0.007762		261	0.01014	0.139
45	0.001882	0.134	272	0.02781	0.140
47	-0.002226	0.134	281	0.04336	0.140
49	-0.00694	0.134	292	0.06312	0.140
50	-0.01196	0.134	294	0.06665	0.140
62	-0.04906	0.134	300	0.07676	0.140
73	-0.08947	0.134	320	0.1163	0.141
84	-0.1175	0.135	331	0.139	0.141
95	-0.1272	0.135	341	0.1581	0.141
108	-0.1279	0.135	352	0.1822	0.142
110	-0.1277	0.136	361	0.202	0.142
121	-0.1272	0.136	370	0.2219	0.142
132	0.1096	0.136	380	0.2419	0.142
142	-0.09723	0.136	391	0.2666	0.143
153	-0.1216	0.137	402	0.2919	0.143
164	-0.1139	0.137	415	0.3218	0.143
177	-0.09923	0.137	426	0.348	0.143
188	-0.0872	0.138	439	0.3784	0.144
199	-0.07429	0.138	441	0.383	0.144
210	-0.06056	0.138	458	0.4237	0.144
229	-0.03636	0.139	469	0.4507	0.144
246	-0.01269	0.139	471	0.4555	0.144
251	0.01010	0.139	482	0.4824	0.145
255	0.01012	0.139	491	0.5059	0.145
259	0.01013	0.139	500	0.5193	0.145

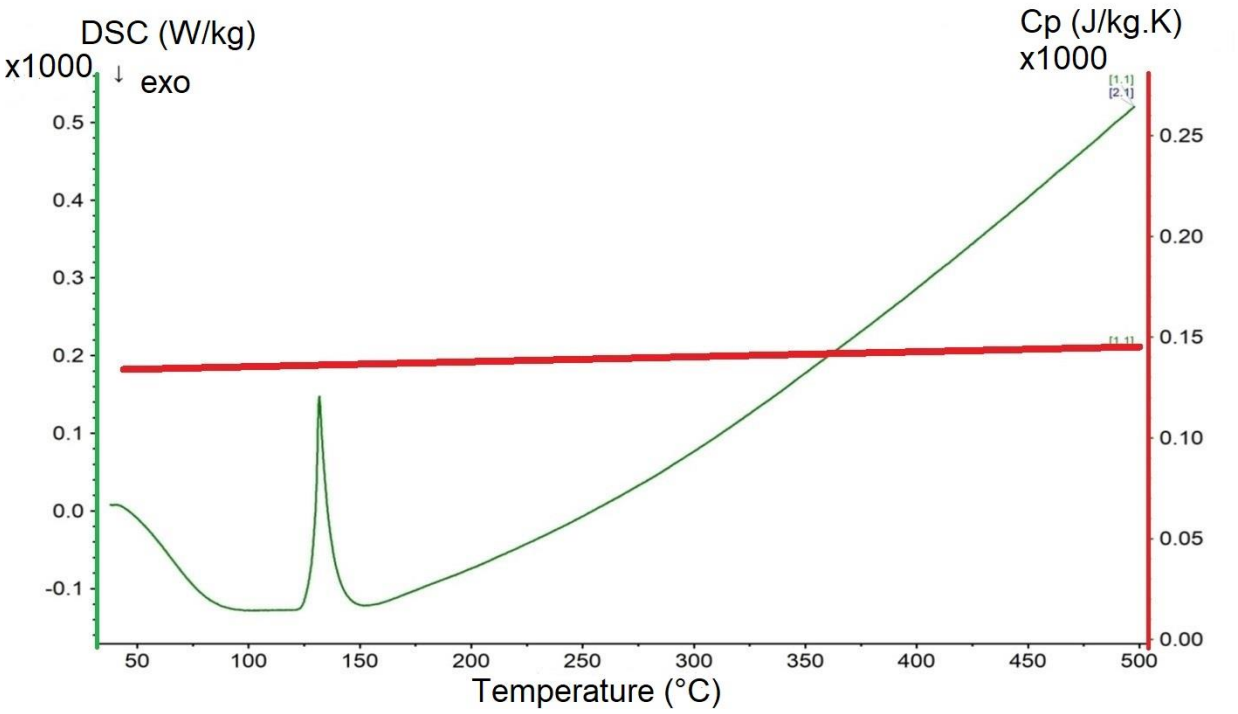

Fig. 12 DSC experiment test 8 and 9 measurement of specific heat capacity with a heating rate of 5 K/min; Argon gas environment.

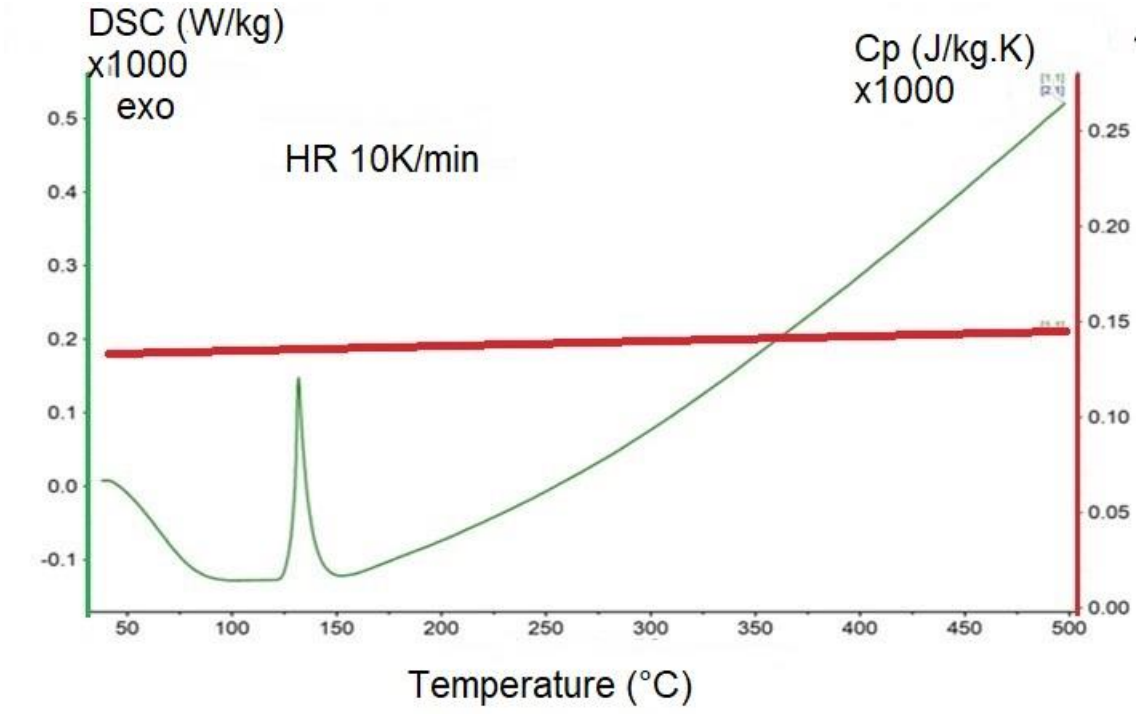

Fig. 13 DSC experiment test 8 and 9 measurement of specific heat capacity with a heating rate of 10 K/min; Argon gas environment.

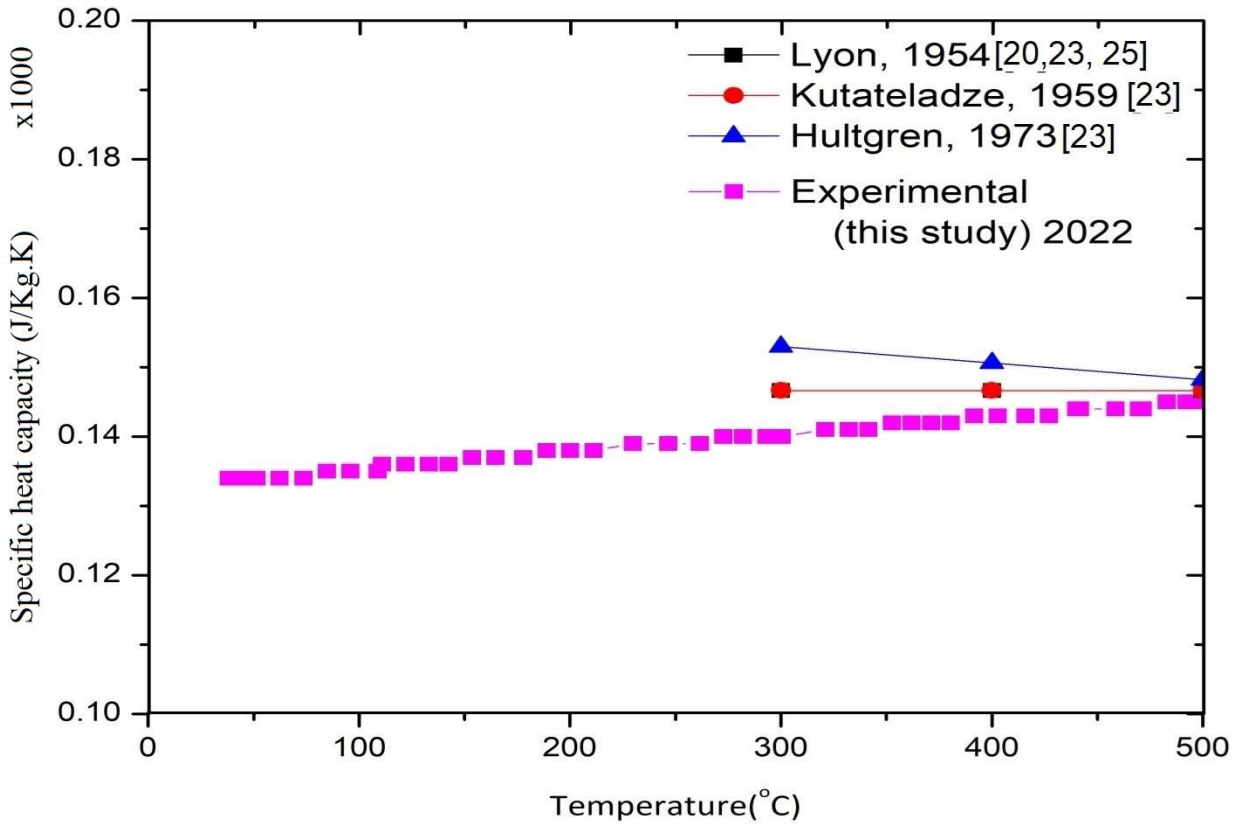

Fig. 14 Comparison of the experimentally determined LBE specific heat capacity with published data [20,23 and 25]

4.5 Test 12

More comprehensive temperature ranges were used in the subsequent experiment, but it was only partially successful (failed at higher temperatures) (after 1300^{o}C). The investigation results demonstrate that pressure develops rapidly at around 800^{o}C when evaporation is prevalent in the furnace compartment, thermocouple, and crucible. Figure 15 shows the characteristics of this experiment test 12. Figure 15 indicates that the DSC output change is consistent over time and smaller in magnitude up to a temperature of around 1300^{o}C. The DSC output suddenly increases with very high rate after a temperature of roughly 1300^{o}C, although temperature also lose control and increased abruptly to emergency temperature even though we have programmed the temperature increase rate limit to 20 K/min.

The observed temperature is notably lower than the boiling temperature of LBE and the designated temperature limit of the equipment. This discrepancy may be attributed to substantial evaporation, despite the boiling temperature of LBE being approximately 1600°C [21]. At this stage, the device's display indicator displays a message that contact has broken between the thermocouple and the sample crucible, and we promptly stop the experiment.

This test provides crucial information for designing future experiments to control evaporation and buckling in the DSC apparatus at higher temperatures. This test also demonstrates the need

for accurate temperature management and control mechanisms at higher temperatures to prevent any emergencies that may damage the equipment. Tables 8, 9, and 10 provide the specifics of test 8 parameters, sample and reference crucibles, and temperature program. While Table 11 contains all the information relevant to experimental test 12,

Table 8 Details of components and parameters during experimental test 12

Instrument	NETZSCH DSC 404F3 DSC404F3A-0272-M
Method used	new measurement
Date/Time	25/05/2022 09:47:55 (UTC+2)
End Date/Time	25/05/2022 10:53:56 (UTC+2)
Laboratory	ENEA
Measurement Type	Sample
Temperature Calibration	TCALZERO.TMX
Sensitivity	24-05-2022 14:26
Crucible	Al_2O_3 85 µl, open
Remark	
Furnace	SiC S
Sample carrier	DSC Cp S
Measurement End	Reset: Furnace or sample overheating
Furnace TC	S
Sample TC	S

Table 9 Sample crucible parameters details for experimental test 12

Sample identity	PbBi
Sample Mass	292.8 mg
Crucible	Al_2O_3 85 µl, open
Crucible Mass	132.9 mg
Reference name	Al_2O_3
Reference Mass	0 mg
Reference Crucible Mass	132.9 mg
Material	Al
Sample determination mode	Manual

Table 10 Temperature programme for experimental test 12

Num	Mode	Temp. °C	HR K/min	Acq.Rate pts/min	Duration hh:mm	STC	P2: Ar	PG: Ar
0	Start	20.0				1	20.0	50.0
1	Dynamic	1500.0	20.000	200.00	01:14	1	20.0	50.0
2	Isothermal	1500.0		300.00	00:01	1	20.0	50.0
3	Emergency	1510.0					20.0	50.0
4	Final stand-by heating	20.0	40.000		00:37	1	20.0	50.0
5	Final stand-by isothermal	20.0			02:00	1	20.0	50.0

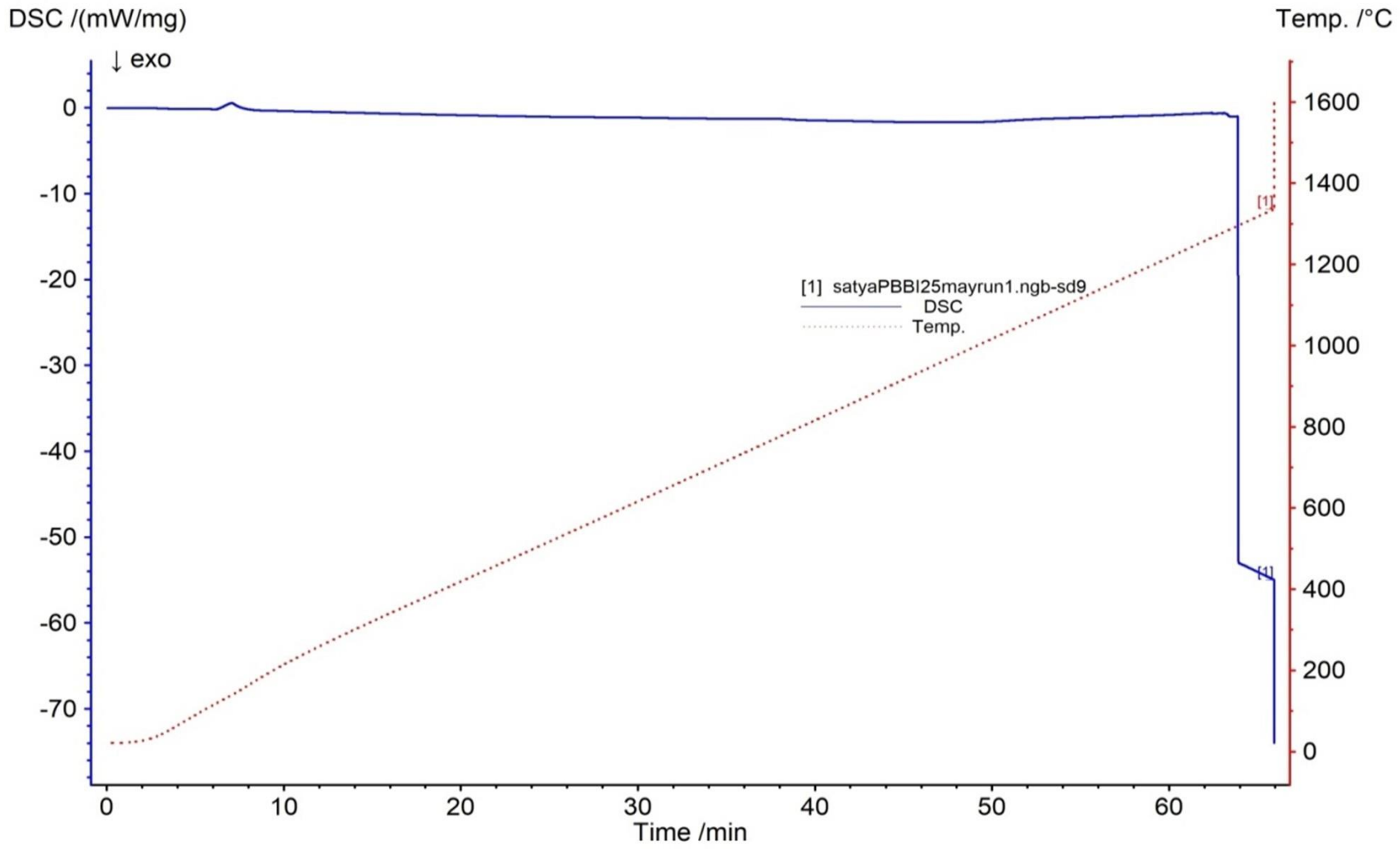

Fig. 15 Detail profile of DSC output and temperature program during Test 12

Table 11 Data related to experimental test 12.

Temp. °C	Time min	DSC mW/mg	Sensitivity µV/mW	Segment
22	0.0	-0.004086	0.4222	1
29	2.3	-0.02077	0.421	1
78	4.5	-0.1508	0.4124	1
133	6.8	0.3794	0.4009	1
192	9.1	-0.3345	0.387	1
245	11.3	-0.4409	0.3732	1
293	13.6	-0.5551	0.36	1
338	15.9	-0.668	0.3472	1
383	18.2	-0.7741	0.3346	1
427	20.4	-0.8811	0.3221	1
472	22.7	-0.9684	0.3098	1
517	25.0	-1.039	0.2977	1
561	27.2	-1.09	0.2861	1
606	29.5	-1.136	0.275	1
652	31.8	-1.193	0.2645	1
697	34.0	-1.25	0.2545	1
742	36.3	-1.26	0.2452	1
788	38.6	-1.345	0.2364	1
833	40.9	-1.498	0.2282	1
879	43.1	-1.584	0.2205	1
924	45.4	-1.666	0.2133	1
970	47.7	-1.687	0.2064	1
1015	49.9	-1.612	0.1998	1
1061	52.2	-1.351	0.1935	1
1106	54.5	-1.185	0.1872	1
1152	56.8	-1.045	0.181	1
1197	59.0	-0.9042	0.1748	1
1243	61.3	-0.7099	0.1684	1
1289	63.6	-1.026	0.1621	1
1334	65.8	-54.87	0.1556	1

5. Uncertainties of measured and calculated parameters

Uncertainty is used to demonstrate the reliability of instrument findings during different experiments, and uncertainty examination may provide a rational and scientific assessment of the precision of data collected [42 and 43]. As a rule, the more uncertain a measurement is, the more likely it will be inaccurate and the less reliable. The melting temperature and the latent heat of melting, solidification temperature and the latent heat of solidification, and specific heat capacity of LBE experimental data are associated with uncertainty estimation [43]. In experimentation, the following are the main two different types of uncertainty: standard uncertainty of category 1

also called random errors., which is subjected to statistical analysis of collections of experimental measurements, and conventional uncertainty of class 2 also called systematic errors, which is rooted in quality assurance qualifications of devices.

Multiple repetitive experimental tests were conducted to investigate the melting, solidification, and specific heat of LBE. However, it should be noted that only the most favorable test results are reported in this manuscript. By performing a series of experiments, the aim was to ensure reliable and consistent data collection while eliminating potential anomalies or experimental errors. The selected test results were deemed the most representative and indicative of the desired phenomena under investigation.

The typical uncertainty of category 1 (random uncertainty), produced by randomness in experimental reproducibility, may be represented as in equation (1)

$$u_1(z) = \frac{\sigma(z)}{\sqrt{N}} \dots\dots (1)$$

as a percentage of average value of parameter, the relative uncertainty of type 1 (relative random uncertainty) is given by equation (2)

$$u_{1r}(z) = \frac{u_1(z)}{\bar{z}} \times 100\% \dots\dots (2)$$

Where in equation (1) and (2) $u_1(z)$ and $u_{1r}(z)$ are uncertainties of type 1 and relative uncertainties of type 1 respectively in parameter Z, $\sigma(z)$ is the standard deviation, N is the number of measurements of parameter z and $\bar{z}$ is the average value of the parameter.

where standard deviation is calculated by the formula given by equation (3)

$$\sigma(z) = \sqrt{\frac{1}{N-1}\sum_{i=1}^{N}[z(i) - \bar{z}]^2} \dots. (3)$$

Using the equations (1)- (3) the relative uncertainties of type 1 (random uncertainty) in melting point of LBE is 0.1%, and 0.245% in latent heat of melting, while the relative uncertainties of type 1 in solidification point of LBE is 0.106% and 0.41% in latent heat of solidification. The specific heat capacity has 0.24% of relative uncertainties of type 1.

Additionally, the instrument-caused uncertainty is category 2 reference uncertainty (systematic uncertainty). The reliability of the DSC measuring device is around +/-3% (this value is provided by the manufacturer and is reported in the operational manual) [44].

Given that it is susceptible to being uniformly distributed, the following equations (4) and (5) describes the category 2 reference uncertainty:

$$u_2(z) = \frac{Hw}{K} \ldots\ldots (4)$$

$$u_{2r}(z) = \frac{u_2(z)}{\bar{z}} \times 100\% \ldots\ldots (5)$$

here in equations (4) and (5) 'Hw' is the interval half width, K is the coverage factor, $u_2(z)$ is uncertainty type 2 and $u_{2r}(z)$ is relative uncertainties of type 2 (relative systematic uncertainty).

In uncertainty analysis, the interval of half-width and the coverage factor are essential concepts used to quantify and represent the uncertainty associated with a measurement or calculation. Below is the explanation of these factors:

The interval of half-width, also known as the confidence interval or uncertainty interval, represents the range within which the true value of a parameter is expected to lie with a certain level of confidence. It is typically expressed as a symmetric range around the estimated value and is characterized by a half-width.

The coverage factor is a statistical term relating to the desired confidence level in an uncertainty analysis. It represents the standard deviations needed to encompass the desired confidence level. The coverage factor is often denoted by the symbol "k."

Commonly used coverage factors include k=2 for a 95% confidence level and k=3 for a 99% confidence level. These values are derived from statistical distributions, such as the normal distribution, and account for the variability and uncertainty in the measurements or calculations.

When calculating the interval of half-width, the coverage factor is multiplied by the standard deviation (or standard uncertainty) of the measurement or calculation to determine the range that captures the desired confidence level.

It's important to note that the specific choice of coverage factor depends on the desired level of confidence and the statistical assumptions made in the uncertainty analysis. Different fields or applications may have varying conventions for selecting the appropriate coverage factor.

So, by utilizing equations (4) and (5) with coverage factor K=2,) and coverage bandwidth of 95%, the relative uncertainties of type 2 (systematic uncertainty) in the melting point of LBE are 1.12% and 1.45% in the latent heat of melting. In comparison, the relative uncertainties of type 1 in the solidification point of LBE are 1.2% and 1.61% in the latent heat of solidification. The specific heat capacity has 1.54% of relative uncertainties of type 2.

Uncertainty studies showed that the highest calculated composite uncertainty (which is defined by combined uncertainty of type 1 and type 2) is given by equation (6)

$$u_c(z) = \sqrt{u_{1r}(z)^2 + u_{2r}(z)^2} \ldots\ldots (6)$$

in the melting point of LBE is 1.12% and 1.47% in latent heat of melting, while in the solidification point of the LBE it is 1.2% and 1.66% in latent heat of solidification. The specific heat capacity has a composite uncertainty of 1.56%.

6. Conclusions

The lead-bismuth eutectic's critical thermal characteristics have been determined by several experiments at the established DSC facility at ENEA Brasimone, Italy. In comparison to the results of the literature, the experimental test results, and uncertainty assessment reveal that the properties obtained have extremely low uncertainties and acceptable accuracy. This exercise helped to rebuild the data libraries for lead-based coolant for the various nuclear systems with the most recent, accurate, and advanced techniques like DSC since there are many uncertainties in the literature, which have been discussed in the introduction of this manuscript. This exercise also helps thermal-hydraulic codes predict system responses more accurately. The ultimate purpose of the DSC facility established at ENEA, Brasimone, is to precisely determine the lead-lithium thermal characteristics, which have been used for various system code model validations (like SIMMER-III), to complete the safety analysis of the Water cool lithium lead (WCLL) blanket during transients. In this study, a significant amount of practice, methods, experience, and methodologies have been established to accomplish the next step of measuring the lead-lithium properties stated above.

The main concluding points of this study are listed below:

1. To guarantee the reliability of the measuring instrument, temperature calibration and sensitivity calibration are performed before the experimental test. Different reference sample materials are utilized for temperature and sensitivity calibration, each with a distinct melting point and melting enthalpy. In contrast, Indium is the most appropriate material for the measurement of LBE as its melting point is most comparable to the LBE theoretical melting point. For the calibration of latent heat and heat capacity, platinum is used as its heat capacity is comparable to LBE.

2. The measured thermal properties of LBE are the melting point of 124.36^{o}C, latent heat of melting of 37.82 J/g, solidification point of the LBE of 140.35^{o}C, latent heat of solidification of 36.65 J/g, and specific heat capacity is measured for large temperature span (21^{o}C to 500^{o}C) with high accuracy and appropriately defined environmental conditions compared to literature values.

3. Studies on uncertainty reveal that the most significant computed composite uncertainty (defined by the combined value of type 1 and type 2 uncertainties) for the LBE's melting point and solidification point is 1.12 percent and 1.2 percent in latent heat of melting and solidification, respectively. The overall uncertainty for the specific heat capacity is 1.56 percent.

4. The additional experiment was tried across a more comprehensive temperature range but was partial (failed at higher temperatures after 1300^{o}C). The study's findings show that pressure

increases quickly in the furnace compartment, thermocouple, and crucible at temperatures of roughly 800°C when evaporation is predominant. This provides crucial information for designing future experiments to control evaporation and buckling in the DSC apparatus at higher temperatures. This test also demonstrates the need for accurate temperature management at higher temperatures to prevent emergencies that may damage the equipment.

Nomenclature

C_p	specific heat capacity, J/kg K
H_w	interval half width,
K	coverage factor
N	number of measurements of parameter z
$u_1(z)$	uncertainty type 1
$u_{1r}(z)$	relative uncertainties of type 1 (relative systematic uncertainty).
$u_2(z)$	uncertainty type 2
$u_{2r}(z)$	relative uncertainties of type 2 (relative systematic uncertainty).
Z	parameter
$\bar{z}$	average value of the parameter.

Greek Letters

$\sigma(z)$	standard deviation

Acronyms and abbreviations widely used in text and list of references

Acq.Rate	Data acquisition rate (points/min)
ADS	accelerator-driven System
Al	Aluminium
Al_2O_3	Alumina (aluminum oxide)
Ar	Argon gas
Bi	Bismuth
CFD	computational fluid dynamics

CRM	certified reference materials
DEMO	DEMOnstration power plant
DICI-UNIPI	department of Civil and Industrial Engineering, University of Pisa, Pisa Italy
DSC	differential Scanning Calorimetry Equipment and Techniques
ENEA	national agency for new technologies, Brasimone, Italy
exo.	exothermic
HCl	Hydrochloric acid
H_2SO_4	Sulfuric acid
HR	heating rate
HLM	heavy liquid metals
Li	lithium
LFR	lead-cooled fast reactor
LBE	Lead Bismuth Eutectic
LFR	lead-cooled fast reactor
Min	minutes
NaK	sodium–potassium alloy
Num.	Number
Pb	lead
Pb-Bi	lead Bismuth eutectic
Pb-Li	lead lithium eutectic
PG	purge gas
P2	protective gas
REA	research Executive Agency
SiC	silicon-carbide

SIMMER-III	fluid-dynamics code coupled with a structure model and a space-, time- and energy-dependent neutron dynamics model
STC	Sample Thermal Conductivity
Temp.	Temperature
TRL	technology Readiness Level
TC	thermo-Couple
WCLL	water-Cooled Lithium Lead blanket

Subscripts or Superscripts

P	pressure
r	relative uncertainties
1	type 1 uncertainties
2	type 2 uncertainties

Figure caption list

Fig. 1 (a) DSC schematic with various components, (b) Photograph of Complete DSC setup installed at ENEA Brasimone, (c) Photograph of inside the hosting device contains Crucible, heating elements and radiators, (d) NETZSCH-Proteus software installed in windows-based PC with various options, NETZSCH-Proteus

Fig. 2 Sensitivity calibration obtained for alumina crucible and for purge and protection argon gas flow 20 ml/min and 50 ml/min respectively

Fig. 3 Correction type of experiment with empty reference and sample crucible.

Fig. 4 A general Sample + correction measurement test 1 with imported calibration files for temperature and sensitivity

Fig. 5 DSC experiment test 2, measurement of melting point temperature and latent heat of melting with a heating rate of 5 K/min; Argon gas environment and other details are given in figure footer.

Fig. 6 DSC experiment test 3, measurement of melting point temperature and latent heat of melting with a heating rate of 10 K/min; Argon gas environment and other details are given in figure footer

Fig. 7 DSC experiment test 4, measurement of melting point temperature and latent heat of melting with a heating rate of 15 K/min; Argon gas environment and other details are given in figure footer.

Fig. 8 DSC experiment test 5, measurement of melting point temperature and latent heat of melting with a heating rate of 20 K/min; Argon gas environment and other details are given in figure footer.

Fig. 9 Summary of DSC experiment tests 2-5

Fig. 10 DSC experiment test 6, measurement of solidification point temperature and latent heat of solidification with a cooling rate of 10 K/min; Argon gas environment and other details are given in figure footer.

Fig. 11 DSC experiment test 7, measurement of solidification point temperature and latent heat of solidification with a cooling rate of 5 K/min; Argon gas environment and other details are given in figure footer

Fig. 12 DSC experiment test 8 and 9 measurement of specific heat capacity with a heating rate of 5 K/min; Argon gas environment.

Fig. 13 DSC experiment test 8 and 9 measurement of specific heat capacity with a heating rate of 10 K/min; Argon gas environment.

Fig. 14 Comparison of the experimentally determined LBE specific heat capacity with published data [20,23 and 25]

Fig. 15 Detail profile of DSC output and temperature program during Test 12

Table caption list

References

1. Wei, S., Wang, C., Tian, W., Qiu, S., & Su, G. (2019). "Research progress in key thermal-hydraulic issue of lead-based fast reactor." ("Natural circulation capability of Pb-Bi cooled fast reactor: PEACER") Atomic Energy Science and Technology, 53(2), 326. DOI: 10.7538/yzk.2018.youxian.0335.

2. IEA ETP (2022) Clean Energy Technology Guide https://www.iea.org/data-and-statistics/data-tools/etp-clean-energy-technology-guide?search=nuclear

3. Bandini, G., Meloni, P., & Polidori, M. (2011). Thermal-hydraulics analyses of ELSY lead fast reactor with open square core option. Nuclear Engineering and Design, 241(4), 1165-1171. https://doi.org/10.1016/j.nucengdes.2010.04.034.
4. EFDA Fusion Electricity-A roadmap to the realization of fusion energy November 2012 http://users.eurofusion.org/iterphysicswiki/images/9/9b/EFDA_Fusion_Roadmap_2M8JBG_vl_0.pdf.
5. Federici, G.; Bachmann, C.; Biel, W.; Boccaccini, L.; Cismondi, F.; Ciattaglia, S.; Coleman, M.; Day, C.; Diegele, E.; Franke, T.; Grattarola, M.; Hurzlmeier, H.; Ibarra, A.; Loving, A.; Maviglia, F.; Meszaros, B.; Morlock, C.; Rieth, M.; Shannon, M.; Taylor, N.; Tran, M.; You, J.; Wenninger, R.; Zani, L. (2015). Overview of the design approach and prioritization of R&D activities towards an EU DEMO. Fusion Engineering and Design, (109), https://doi.org/10.1016/j.fusengdes.2015.11.050
6. Saraswat, S., P., Cossu, V., Galleni, F., Eboli, M., Nevo, A., Forgione, N., (2023) "Progress towards the Validation of SIMMER-III code model for Lead lithium water chemical interaction," Fusion Engineering and Design. https://doi.org/10.1016/j.fusengdes.2023.113819
7. Saraswat, S., P., Galleni, F., Eboli, M., Nevo, A., Forgione, N., (2022) "Numerical investigation of LIFUS5/Mod3 Series E Experiments Test 5.1 towards thermal-hydraulic system code SIMMER III validation", FMFP-2022, 9th International and 49th National conference of FMFP, December 14-16, 2022, IIT Roorkee, India. https://easychair.org/publications/preprint/ZlmB
8. Saraswat, S., P., Ray, D., Mishra, G., Yadav, D., Bhadouria, V., Munshi, P., and Allison, C.

(2021). "Thermal-hydraulic Safety Assessment of Full-Scale ESBWR Nuclear Reactor Design." ASME. ASME J of Nuclear Rad Sci. https://doi.org/10.1115/1.4052014

9. Ray, D., Saraswat, S., P., Kumar, M., Singh, O., & Munshi, P. (2022). Build Up and Characterization of Ultraslow Nuclear Burn-Up Wave in Epithermal Neutron Multiplying Medium. Journal of Nuclear Engineering and Radiation Science, 8(2), 021501. https://doi.org/10.1115/1.4049727
10. Saraswat, S., P., Ray, D., Munshi, P., & Allison, C. (2019). Analysis of loss of heat sink for ITER divertor cooling system using modified RELAP/SCDAPSIM/MOD 4.0. Journal of Nuclear Engineering and Radiation Science, 5(4), 042202. https://doi.org/10.1115/1.4042707.
11. Saraswat, S., P., Munsh, P., Khanna, A., & Allison, C. (2018). Thermal hydraulic safety assessment of llcb test blanket system in ITER using modified RELAP/SCDAPSIM/MOD4. 0 code. Journal of Nuclear Engineering and Radiation Science, 4(2), 021001. https://doi.org/10.1115/1.4038823
12. Saraswat, S., P., Munshi, P., Khanna, A., & Allison, C. (2017). Ex-Vessel Loss of Coolant Accident Analysis of ITER Divertor Cooling System Using Modified RELAP/SCADAPSIM/Mod 4.0. Journal of Nuclear Engineering and Radiation Science, 3(4), 041009. https://doi.org/10.1115/1.4037188
13. Saraswat, S., P., Munshi, P., Khanna, A., & Allison, C. (2017). Thermal Hydraulic and Safety Assessment of First Wall Helium Cooling System of a Generalized Test Blanket System in ITER Using RELAP/SCDAPSIM/MOD4. 0 Code. Journal of Nuclear Engineering and Radiation Science, 3(1), 014503. https://doi.org/10.1115/1.4034680.
14. Saraswat, S., P., Munshi, P., Khanna, A., Allison, C. (2020) "Thermal hydraulics of loss of heat sink accident of Indian test blanket system in ITER," International Youth Nuclear Congress (IYNC), 2020, March 10-12, 2020, Sydney. https://drive.google.com/file/d/1eW7Czet2dcKaTZn4KCJB1Ut-ZmgeGGLz/view?pli=1
15. Saraswat, S., P., Munshi, P., Khanna, A., & Allison, C. (2020). Thermal Hydraulic Analysis of in-Vessel Loss of Coolant Accident and Loss of Flow Accident of First Wall Helium Cooling System of Generalized LLCB TBS in ITER Using Modified RELAP/SCDAPSIM MOD4. 0. EasyChair, Kanpur, India, Paper, (2657), 14. https://easychair.org/publications/preprint/RZL6
16. Saraswat, S., P., Munshi, P., Khanna, A., & Allison, C. (2020). In-Vessel Loss of coolant accident assessment of a generalized LLCB TBS in ITER using RELAP/SCDAPSIM Code. EasyChair, Kanpur, India, Paper, (2757). https://www.academia.edu/66850345/In_Vessel_Loss_of_coolant_accident_assessment_of_a_generalized_LLCB_TBS_in_ITER_using_RELAP_SCDAPSIM_Code
17. Martelli, D., Venturini, A., & Utili, M. (2019). Literature review of lead-lithium thermophysical properties. Fusion Engineering and Design, 138, 183-195. https://doi.org/10.1016/j.fusengdes.2018.11.028
18. Sobolev, V. (2007). Thermophysical properties of lead and lead–bismuth eutectic. Journal of nuclear materials, 362(2-3), 235-247. https://doi.org/10.1016/j.jnucmat.2007.01.144

19. Pioro, I., & Duffey, R. (2019). Current and future nuclear power reactors and plants. In Managing Global Warming (pp. 117-197). Academic Press. https://doi.org/10.1016/j.jnucmat.2007.01.144
20. Lyon, R.N. (Ed.) (1954), Liquid Metals Handbook, 2nd Ed., Report NAVEXOS P-733, Atomic Energy Commission and Dept. of the Navy, Washington, USA.
21. Lyon, R. N., & Poppendiek, H. (1951). Liquid-metal heat transfer. Liquid-metals Handbook, 184.
22. Li, N., Wang, Y., Liu, Q., & Peng, H. (2022). Evaluation of thermal-physical properties of novel multicomponent molten nitrate salts for heat transfer and storage. Energies, 15(18), 6591. https://doi.org/10.3390/en15186591
23. Fazio C. (2016) Handbook on Lead-bismuth Eutectic Alloy and Lead Properties, Materials Compatibility, Thermal-hydraulics and Technologies; Paris (France): OECD; 2016. p. 17-27. JRC100764. https://publications.jrc.ec.europa.eu/repository/handle/JRC100764
24. Mantell, L. (Ed.) (1958), Engineering Material Handbook, MacGraw-Hill, USA. https://iopscience.iop.org/article/10.1149/1.2428814/pdf
25. Lyon, R.N. (1960), "Liquid Metals", Chapter 49 in: Reactor Handbook, 2nd Ed.(rev., enl.), Vol. I, Materials, Sect. F (Coolant Materials), C.R. Tipton, Jr. (Ed.), Inter science Publishers, New York, USA. https://www.osti.gov/biblio/4377939
26. Zhang, J., Kapernick, R. J., McClure, P. R., & Trapp, T. J. (2013). Lead–bismuth eutectic technology for Hyperion reactor. Journal of nuclear materials, 441(1-3), 644-649. https://doi.org/10.1016/j.jnucmat.2013.04.079
27. Fazio, C., Sobolev, P., Aerts, A., Gavrilov, S., Lambrinou, K., Schuurmans, P., ... & Hwang, I. S. (2015). Handbook on lead-bismuth eutectic alloy and lead properties, materials compatibility, thermal-hydraulics and technologies-2015 edition (No. NEA--7268). Organisation for Economic Co-Operation and Development. https://inis.iaea.org/search/search.aspx?orig_q=RN:46133907
28. Roelofs, F., Shams, A., Otic, I., Böttcher, M., Duponcheel, M., Bartosiewicz, Y., & Cheng, X. (2015). Status and perspective of turbulence heat transfer modelling for the industrial application of liquid metal flows. Nuclear Engineering and Design, 290, 99-106. https://doi.org/10.1016/j.nucengdes.2014.11.006
29. Hultgren, R., Desai, D., Hawkins, T., Gleiser, M., & Kelley, K. (2007). Selected Values of the Thermodynamic Properties of Binary Alloys (ASM, Metals Park, OH, 1973). https://apps.dtic.mil/sti/citations/ADD095435
30. Plevachuk, Y., Sklyarchuk, V., Eckert, S., & Gerbeth, G. (2008). Some physical data of the near eutectic liquid lead–bismuth. Journal of Nuclear Materials, 373(1-3), 335-342. https://doi.org/10.1016/j.jnucmat.2007.06.014
31. Barrado, I., Conde, E., Fernández, M., Gómez-Salazar, M., Quejido, A., & Quiñones, J. (2012). Towards the development of technical specifications for the production of lithium–lead alloys for the ITER HCLL TMB. Fusion Engineering and Design, 87(7-8), 1297-1300. https://doi.org/10.1016/j.fusengdes.2012.02.120
32. Sobolev, V. (2007). Thermophysical properties of lead and lead–bismuth eutectic. Journal of nuclear materials, 362(2-3), 235-247.

https://doi.org/10.1016/j.jnucmat.2007.01.144
33. Lipchitz, A., Harvel, G., & Sunagawa, T. (2022). Thermophysical Characteristics of Liquid Metal In-Bi-Sn Eutectic (Field's Metal) as a Similarity Coolant. Journal of Nuclear Engineering and Radiation Science, 8(3), 031301. https://doi.org/10.1115/1.4053632
34. Sobolev, V. (2005). MYRRHA ADS DATABASE: Part I. Thermophysical properties of molten lead-bismuth eutectic. Version 1. https://www.osti.gov/etdeweb/biblio/20902510
35. Morita, K., Maschek, W., Flad, M., Yamano, H., & Tobita, Y. (2006). Thermophysical properties of lead-bismuth eutectic alloy in reactor safety analyses. Journal of nuclear science and technology, 43(5), 526-536. https://www.tandfonline.com/doi/abs/10.1080/18811248.2006.9711131
36. TECDOC-1289 (2002), Comparative Assessment of Thermophysical and Thermohydraulic Characteristics of Lead, lead-bismuth and Sodium Coolants for Fast Reactors, IAEA, Vienna. https://www-pub.iaea.org/MTCD/Publications/PDF/te_1289_prn.pdf
37. Montanari, R., Varone, A., Gregoratti, L., Kaciulis, S., & Mezzi, A. (2019). Lead-Bismuth Eutectic: Atomic and Micro-Scale Melt Evolution. Materials, 12(19), 3158. https://doi.org/10.3390/ma12193158
38. Wang, L., Zhang, Y., Huang, R., Li, Q., Peng, T., & Hong, G. (2020). Measurement and analysis of specific heat capacity of lead-bismuth eutectic. Progress in Nuclear Energy, 123, 103284. https://doi.org/10.1016/j.pnucene.2020.103284
39. Popa, K., Beneš, O., Staicu, D., Griveau, C., Colineau, E., Raison, E., & Konings, M. (2016). Thermal properties of PbUO4 and Pb3UO6. Journal of Nuclear Materials, 479, 189-194. https://doi.org/10.1016/j.jnucmat.2016.07.021
40. Larouche, D., Laroche, C., & Bouchard, M. (2003). Analysis of differential scanning calorimetric measurements performed on a binary aluminium alloy. Acta Materialia, 51(8), 2161-2170. https://doi.org/10.1016/S1359-6454(03)00003-X
41. Varghese, N., Vivekchand, C., Govindaraj, A., & Rao, R. (2008). A calorimetric investigation of the assembly of gold nanorods to form necklaces. Chemical Physics Letters, 450(4-6), 340-344. https://doi.org/10.1016/j.cplett.2007.11.022
42. Sarge, M., Poeûnecker, W., 1999. The influence of heat resistances and heat transfers on the uncertainty of heat- capacity measurements by means of differential scanning calorimetry (DSC). Thermochim. Acta 329, 17–21 https://doi.org/10.1016/S0040-6031(99)00007-6
43. Rudtsch, S., 2002. Uncertainty of heat capacity measurements with differential scanning calorimeters. Thermochimica acta, 382(1-2), pp.17-25. https://doi.org/10.1016/S0040-6031(01)00730-4
44. NETZSCH, Gerätebau GmbH, (2018), Software Manual, DSC 404 - Pegasus F1 & F3, 38080 / Version 1.